

0.2

~~CONFIDENTIAL~~

NACA RM L57G25

NACA

RESEARCH MEMORANDUM

LATERAL STABILITY INVESTIGATION AT MACH NUMBERS FROM
0.8 TO 1.7 OF TWO ROCKET-BOOSTED MODELS OF
AN AIRPLANE CONFIGURATION WITH A
45° SWEEP WING AND A LOW
HORIZONTAL TAIL

By John C. McFall, Jr., Jesse L. Mitchell,
and A. James Vitale

Langley Aeronautical Laboratory
Langley Field, Va.

LIBRARY COPY

OCT 2 1957

LANGLEY AERONAUTICAL LABORATORY
LIBRARY, NACA
LANGLEY FIELD, VIRGINIA

Nonconfidential
78 1-22-58

CLASSIFIED DOCUMENT

This material contains information affecting the National Defense of the United States within the meaning of the espionage laws, Title 18, U.S.C., Secs. 793 and 794, the transmission or revelation of which in any manner to an unauthorized person is prohibited by law.

NATIONAL ADVISORY COMMITTEE FOR AERONAUTICS

WASHINGTON

September 30, 1957

~~CONFIDENTIAL~~



NATIONAL ADVISORY COMMITTEE FOR AERONAUTICS

RESEARCH MEMORANDUM

LATERAL STABILITY INVESTIGATION AT MACH NUMBERS FROM
0.8 TO 1.7 OF TWO ROCKET-BOOSTED MODELS OF
AN AIRPLANE CONFIGURATION WITH A
45° SWEEP WING AND A LOW
HORIZONTAL TAIL

By John C. McFall, Jr., Jesse L. Mitchell,
and A. James Vitale

SUMMARY.

Rocket-boosted free-flight tests of two models of an airplane configuration having a 45° swept wing and a low horizontal-tail position have provided lateral stability derivatives and control effectiveness data for a Mach number range from 0.8 to 1.7. The experimental lateral stability derivatives presented are corrected to rigid conditions and compared with theoretically calculated rigid derivatives. The results are presented without detailed analysis.

INTRODUCTION

A general research program investigating the longitudinal stability and control effectiveness of airplane configurations in rocket-boosted free flight has been conducted by the National Advisory Committee for Aeronautics over the past several years (refs. 1 to 4). Some lateral stability data have been obtained as secondary results of these investigations (ref. 5). Since then some airplane configurations have been flown primarily to determine lateral stability characteristics (refs. 6 to 8). This paper presents the results obtained from the flight tests of two rocket-boosted models of an airplane configuration instrumented and pulse-control disturbed to provide lateral stability and control effectiveness data over a range of Mach numbers from 0.8 to 1.7 and Reynolds numbers from 3×10^6 to 11×10^6 based on the wing mean aerodynamic chord. The models of this investigation had 45° swept wings of aspect ratio 4.0 and taper ratio 0.3 with a low horizontal-tail position.

~~CONFIDENTIAL~~

Both models were disturbed in coasting flight; one by abrupt movements of a differentially deflected horizontal tail and the other by deflections of a rudder. Analysis of the motions of the models following the control deflections by the time-vector methods discussed in references 6 to 9, provided the lateral stability and control effectiveness data presented herein. The control effectiveness data from the differentially deflected horizontal-tail model have been reported in reference 10. The experimental lateral stability derivatives reported herein are corrected to rigid conditions and compared with theoretically calculated rigid derivatives with no detailed analysis.

SYMBOLS

The measured quantities and aerodynamic derivatives of this investigation are referenced to the body axis system illustrated in figure 1.

a	damping factor, $\frac{-0.693}{T_{1/2}}$
a_l	longitudinal accelerometer reading, positive in the positive X-direction, g units
a_n	normal accelerometer reading, positive in the negative Z-direction, g units
a_t	transverse accelerometer reading, positive in the positive Y-direction, g units
b	wing span, ft
C_c	chord-force coefficient, $-a_l \frac{W}{qS}$
C_l	rolling-moment coefficient, $\frac{\text{Rolling moment}}{qSb}$
C_N	normal-force coefficient, $a_n \frac{W}{qS}$
C_n	yawing-moment coefficient, $\frac{\text{Yawing moment}}{qSb}$
C_Y	lateral-force coefficient, $a_t \frac{W}{qS}$
C	coefficient

\bar{c}	mean aerodynamic chord of the wing, ft
c	chord, ft
cps	cycles per second
g	acceleration of gravity, 32.2 ft/sec ²
I_X	moment of inertia about X-axis, slug-ft ²
I_Y	moment of inertia about Y-axis, slug-ft ²
I_Z	moment of inertia about Z-axis, slug-ft ²
I_{XZ}	product of inertia, $\frac{1}{2} (I_Z - I_X) \tan 2\epsilon$, slug-ft ²
i_t	horizontal-tail incidence (parallel to free stream, positive for trailing edge down, and measured in plane parallel to plane of symmetry), deg
i_{td}	differential-tail incidence (i_t of left tail - i_t of right tail), deg
K	elasticity correction factor, $C_{rigid} = KC_{flexible}$
l	length, ft
M	Mach number
m	mass, slugs
P	period of oscillation, sec
p	static pressure, lb/sq ft; or roll velocity, $\dot{\phi}$, radians/sec
q	dynamic pressure, lb/sq ft
R	Reynolds number, based on \bar{c}
r	yawing velocity, radians/sec
S	wing area, sq ft
$T_{1/2}$	time for oscillation to damp to one-half amplitude, sec

t	time, sec
V	velocity, ft/sec
W	weight, lb
X, Y, Z	coordinate axes
α	angle of attack, deg or radians
β	angle of sideslip, deg or radians
ϵ	inclination of principal axis, deg
δ	angular control displacement, deg
η	lateral distance along Y-axis in wing semispans, $\frac{y}{b/2}$
$\frac{\theta}{l}$	local streamwise wing twist angle per unit load, radians/lb
λ_1	damping-in-roll root
ϕ	roll angle, deg or radians
ψ	yaw angle, deg or radians
ω	oscillation frequency, radians/sec
Ω_{C_Y}	phase angle by which C_Y leads β , deg
$\Omega_{\dot{r}}$	phase angle by which \dot{r} leads β , deg
Ω_p	phase angle by which p leads β , deg
Subscripts:	
r	rudder
0	sea-level conditions
β	refers to oscillation in sideslip

A single dot over a symbol indicates the derivative of the quantity with respect to time; a double dot represents the second derivative with

respect to time. Amplitude ratios of the oscillatory components of the motion are designated as $\left| \frac{C_Y}{\beta} \right|$, $\left| \frac{p}{\beta} \right|$, and so forth. The static stability derivatives are indicated in the following manner: $C_{Y\beta} = \frac{\partial C_Y}{\partial \beta}$ and so forth, whereas the rotary and acceleration derivatives are indicated as: $C_{n_r} = \frac{\partial C_n}{\partial \frac{rb}{2V}}$, $C_{n_\beta} = \frac{\partial C_n}{\partial \frac{\beta b}{2V}}$, and so forth.

MODELS AND TESTS

Physical characteristics of the models are shown in figures 2 and 3, and table I. The models flown in this investigation were geometrically the same as the model in a longitudinal stability investigation (ref. 4). An electrohydraulic system was used to move the differentially deflected horizontal tails about the 42-percent chord lines from $i_{td} = 0^\circ$ to $i_{td} = 8^\circ$. For the other model, the rudder was deflected between -0.25° and -8.00° .

The vibrational characteristics of the models were determined by shaking the models mechanically and noting the bending and torsion frequencies. The frequencies recorded were as follows:

Components	Frequency, cps	
	Pulsed horizontal tail model	Pulsed rudder model
Wing: First bending	65.0	68.5
Second bending	233.0	234.0
First torsion	430.0	430.0
Horizontal tail: First bending	102.0	95.0
Vertical tail: First bending	-----	51.5

The structural influence coefficients for the vertical tail were determined experimentally by the methods of reference 11. The influence coefficients for both models were the same and are presented in figure 4.

~~CONFIDENTIAL~~

Influence coefficients for the wing and horizontal tail may be found in references 4 and 10, respectively. These influence coefficients, along with those of figure 4, were used in computing the K-factor elasticity correction (fig. 5) discussed in a subsequent section.

FLIGHT TEST AND INSTRUMENTATION

The models were launched from a mobile launcher (fig. 3(c)) at an angle of 70° from the horizontal. Acceleration to a maximum Mach number of about 1.7 was accomplished with two Deacon solid-propellant rocket motors which separated from the model when burned out. Data were obtained throughout the coasting portion of the flight.

Instrumentation contained in the model measured the following quantities: total pressure, static pressure, normal force, transverse force (at two stations), airflow angularity (pitch and yaw), roll rate, longitudinal force, and angular position of the pulsed controls. Ground instrumentation consisted of tracking radar, velocity radar, and teletype receiving and recording stations. Atmospheric data were obtained with a rawinsonde unit.

The test conditions of the flights (R , V , $\frac{p}{p_0}$, and q) are shown in figure 6 with Reynolds number based on the wing mean aerodynamic chord. The models were tested at the Langley Pilotless Aircraft Research Station at Wallops Island, Va.

ACCURACY AND CORRECTIONS

The estimated accuracy of the basic measurements which affect the stability derivatives is presented at representative Mach numbers for the pulsed rudder model in table II. Approximately the same accuracies will also apply for the pulsed horizontal-tail model.

Following the methods presented in reference 6, the probable accuracy of the stability derivatives as affected by the estimated values of table II are shown in table III as both incremental values and percentage of the measured derivative.

For this analysis, the solution of a vectorial representation of the equations of motion requires that certain derivatives be estimated in order to obtain the other derivatives. The damping-in-roll derivative C_{l_p} (discussed in a subsequent section) was determined for the

pulsed horizontal-tail model from the subsidence of the roll parameter $\frac{pb}{2V}$ and was assumed to be applicable for both models. The effect of the maximum probable error in C_{l_p} on the final derivatives is shown in the lower part of table III. The effect of a 100-percent change in the estimated derivative C_{n_p} is shown in the lower part of table III.

Corrections were made to the measured quantities for small errors caused by instruments which were located off the model center line or off the model center of gravity. The airflow angularity indicator readings were corrected for model pitching and yawing velocities to obtain angles of attack and angles of sideslip, by the method of reference 12.

Corrections were made to the phase angles Ω_p and Ω_{C_Y} for instrument frequency response. These corrections were less than 5° for Ω_p and less than 4° for Ω_{C_Y} .

ANALYSIS

Experimental Results

Time histories of Mach number, rate of roll, angle of attack, and angle of sideslip for the supersonic portion of the flights of both the pulsed horizontal-tail model and the pulsed rudder model are shown in figure 7. The portions of the time histories used in the data analysis are noted on the figure.

For the pulsed horizontal-tail model the high roll-rate oscillations show the coupled motions in angle of attack and angle of sideslip which could not be used for the present analysis.

The roll rate of the pulsed rudder model was relatively low and very little coupling motion was observed. The lateral oscillation β was of greater amplitude than the pitch oscillation α and most of the oscillations had the characteristics of a damped sinusoid and could be used in the present analysis.

The flight-test data obtained in this investigation were analyzed by the time-vector methods discussed and illustrated in detail in references 6 to 9. Basically the data reductions for the models reported herein were as follows: oscillations in β , p , and C_Y following each control deflection were plotted against time and envelopes were

faired about the peak values to aid in determining trim values; trim lines were faired through each oscillation and the times when the oscillations crossed the trim lines were noted; cross plots were made of the trim crossing times against time and fairings of the plotted points were made by using the method of least squares; from these cross plots, phase angles and periods were determined; the time to damp to one-half amplitude was determined from the slope which fitted plots of the amplitude ratios of C_Y , β , and p on semilog paper against time.

The damping-in-roll derivative C_{l_p} was determined for the pulsed horizontal-tail model by finding the damping-in-roll root λ_1 from the subsidence of the roll parameter $\frac{pb}{2V}$ following the control disturbance. The value of steady-state roll parameter was subtracted from the transient response then C_{l_p} was calculated from the damping of the remaining motion through the following approximation:

$$C_{l_p} = \frac{2\lambda_1 I_X}{qSb^2}$$

Theoretical Calculations

The most important contributor to the derivatives is the vertical tail. Calculations were made of the vertical-tail contributions to the derivatives C_{Y_β} , C_{n_β} , C_{n_r} , C_{l_r} , and C_{l_β} by the approximations given by reference 13. The isolated tail lift-curve slope was estimated from slender-body theory of reference 14 for $M = 0.8$ to 1.0 and from reference 15 at supersonic Mach numbers, trailing edge supersonic. The isolated tail lift curve was then multiplied by a factor, obtained from the slender-body theory of reference 14 to account for the end-plate effect of the fuselage and horizontal tail. For this calculation it was assumed that the fuselage was effectively cylindrical in the region of the vertical tail with a radius equal to 0.207 of the tail span. (This radius makes the effective exposed tail area the same as on the model.) The center of pressure was estimated from the same references and was found to be essentially invariant with Mach number for the range of investigation.

The aeroelastic characteristics of the vertical tail were estimated from the influence coefficients of figure 4, the atmospheric test conditions of figure 6, and simple trapezoidal loadings.

The contributions of the various components to the total derivatives were estimated from the sources indicated in the following listing:

Derivatives	References used for estimating contribution of -					Components considered elastic
	Vertical tail	Horizontal tail	Fuselage	Wing	Empennage	
$C_{Y\beta}$	13, 14, 15	10	13, 14			Horizontal and vertical tail
$C_{n\beta}$	13, 14, 15	10	13, 14			Horizontal and vertical tail
C_{n_r}	13, 14, 15	10				Horizontal and vertical tail
$C_{l\beta}$	13, 14, 15	10				Horizontal and vertical tail
C_{l_r}	13, 14, 15	10				Horizontal and vertical tail
C_{l_p}				15, 16, 17, 18, 20	16, 17, 19	Wing

The values of the derivatives were estimated for the rigid configuration and for the elastic model. The ratios of rigid to elastic derivatives were calculated. These ratios presented in figure 5 were used to correct the measured model data for aeroelasticity. No inertial loadings were considered except for rolling inertia effect on rolling moments. The K-factor for the C_{l_p} values includes the aeroelastic effect of rolling moment of inertia. Comparisons between theoretical and experimental derivatives presented herein are for rigid conditions.

PRESENTATION OF DATA

Trim

Faired values of the mean line through the oscillations in angle of attack, angle of sideslip, and the rolling parameter $\frac{pb}{2V}$ are shown in figure 8. The trim values for the pulsed horizontal-tail model were also presented in reference 10 and as stated therein the trim values below $M = 1.0$ indicate the test condition only, since too few cycles were obtained to define trim before the control pulsed to the other stop position. As pointed out in reference 10, the reason for the apparent trim change below $M = 1.0$ is the occurrence of a divergent motion as the rate of roll approaches the natural frequency of the dutch-roll mode of motion. Trim angle of attack was less than 1° for both models throughout the supersonic portion of the flights. This is in agreement with data from the geometrically similar longitudinal stability model of reference 5 with the controls in their undeflected position.

Characteristics of Lateral Oscillations

The frequencies of the lateral oscillations used in the present analysis are shown in figure 9(a). Other characteristics of the lateral motions shown in figures 9(b), 9(c), and 9(d) are the damping factor a ; the amplitude ratios of C_Y , p , and \dot{r} with respect to β ; and the phase angles Ω_{C_Y} , Ω_p , and $\Omega_{\dot{r}}$. A smooth variation with Mach number is noted for all the lateral oscillation characteristics throughout the present test range.

Lateral Stability Derivatives

Typical experimental cross plots of lateral-force coefficient and total yawing-moment coefficient against angle of sideslip are shown in figure 10 for the pulsed horizontal-tail model and in figure 11 for the pulsed rudder model.

Linear fairings were made to permit comparison of slopes with values obtained from the amplitude ratios used in the vector solutions. Figure 12 shows the variation of $C_{Y\beta}$ with Mach number for both models measured from these fairings, the amplitude ratios, and also estimated theoretical values for this configuration. The experimental slopes in figure 12 are corrected for elasticity by the K-factor of figure 5 and the theoretical values were estimated for rigid conditions.

The slopes of the C_n variation with β for both models are plotted against Mach number and compared with the vector solution (assuming $C_{n_p} = 0.15$) in figure 13. Calculated theoretical values of C_{n_β} for this configuration are also shown in figure 13. Both the experimental and theoretical values presented are for rigid conditions.

As mentioned in the section entitled "Experimental Results," the rolling-moment disturbance for the model with the pulsed horizontal tail was such that the subsidence of the roll-rate response could be used to determine the damping-in-roll derivative C_{l_p} . The experimental and theoretical values of C_{l_p} for rigid conditions are presented as a function of Mach number in figure 14.

The lateral stability derivative $C_{l_r} - C_{l_\beta}$ variation with Mach number in figure 15 was obtained from the vector analysis by assuming the C_{l_p} from the subsidence of the rolling parameter to be correct for both models.

The variation of the effective dihedral derivative C_{l_β} with Mach number from the vector solution for both models may be seen in figure 16. The theoretical curve also shown on figure 16 was estimated for rigid conditions and the vector determined points were corrected to rigid conditions by the K-factor of figure 5.

The variation of the damping-in-yaw derivative $C_{n_r} - C_{n_\beta}$ with Mach number from the vector solution corrected to rigid conditions is presented in figure 17. A theoretical curve, obtained as indicated in the section entitled "Theoretical Calculations," is also presented for $C_{n_r} - C_{n_\beta}$ at rigid conditions in figure 17.

Control Effectiveness

The control effectiveness of the pulsed horizontal tail was reported in reference 10. For the rudder model the values of C_{Y_δ} , C_{n_δ} , and C_{l_δ} were determined from the incremental values of the coefficients

following the abrupt control deflection divided by the incremental change in control deflection and are shown in figure 18.

Langley Aeronautical Laboratory,
National Advisory Committee for Aeronautics,
Langley Field, Va., July 9, 1957.

REFERENCES

1. Gillis, Clarence L., Peck, Robert F., and Vitale, A. James: Preliminary Results From a Free-Flight Investigation at Transonic and Supersonic Speeds of the Longitudinal Stability and Control Characteristics of an Airplane Configuration With a Thin Straight Wing of Aspect Ratio 3. NACA RM L9K25a, 1950.
2. Vitale, A. James, McFall, John C., Jr., and Morrow, John D.: Longitudinal Stability and Drag Characteristics at Mach Numbers From 0.75 to 1.5 of an Airplane Configuration Having a 60° Swept Wing of Aspect Ratio 2.24 As Obtained From Rocket-Propelled Models. NACA RM L51K06, 1952.
3. Mitchell, Jesse L.: The Static and Dynamic Longitudinal Stability Characteristics of Some Supersonic Aircraft Configurations. NACA RM L52A10a, 1952.
4. McFall, John C., Jr.: Longitudinal Stability Investigation for a Mach Number Range of 0.8 to 1.7 of an Airplane Configuration With a 45° Swept Wing and a Low Horizontal Tail. NACA RM L55L09, 1956.
5. Purser, Paul E., and Mitchell, Jesse L.: Miscellaneous Directional-Stability Data for Several Airplane-Like Configurations From Rocket-Model Tests at Transonic Speeds. NACA RM L52E06b, 1952.
6. Mitchell, Jesse L., and Peck, Robert F.: Investigation of the Lateral Stability Characteristics of the Douglas X-3 Configuration at Mach Numbers From 0.6 to 1.1 by Means of a Rocket-Propelled Model. NACA RM L54L20, 1955.
7. Gillis, Clarence L., and Chapman, Rowe, Jr.: Effect of Wing Height and Dihedral on the Lateral Stability Characteristics at Low Lift of a 45° Swept-Wing Airplane Configuration As Obtained From Time-Vector Analyses of Rocket-Propelled-Model Flights at Mach Numbers From 0.7 to 1.3. NACA RM L56E17, 1956.
8. D'Aiutolo, Charles T., Willoughby, William W., and Coltrane, Lucille C.: Free-Flight Experience of the Lateral Stability Characteristics at Low Lift of a 45° Swept-Wing Rocket-Propelled Model Equipped With a Nonlinear Yaw-Rate Damper System at Mach Numbers From 0.76 to 1.73. NACA RM L56L18, 1957.
9. Wolowicz, Chester H.: Time-Vector Determined Lateral Derivatives of a Swept-Wing Fighter-Type Airplane With Three Different Vertical Tails at Mach Numbers Between 0.70 and 1.48. NACA RM H56C20, 1956.

10. Mitchell, Jesse L., and Vitale, A. James: Free-Flight Investigation of the Control Effectiveness of a Differentially Deflected Horizontal Tail at Mach Numbers From 0.8 to 1.6. NACA RM L56B20, 1956.
11. Vitale, A. James: Effects of Wing Elasticity on the Aerodynamic Characteristics of an Airplane Configuration Having 45° Sweptback Wings As Obtained From Free-Flight Rocket-Model Tests at Transonic Speeds. NACA RM L52L30, 1953.
12. Ikard, Wallace L.: An Air-Flow-Direction Pickup Suitable for Telemetering Use on Pilotless Aircraft. NACA TN 3799, 1956. (Supersedes NACA RM L53K16.)
13. Campbell, John P., and McKinney, Marion O.: Summary of Methods for Calculating Dynamic Lateral Stability and Response and for Estimating Lateral Stability Derivatives. NACA Rep. 1098, 1952. (Supersedes NACA TN 2409.)
14. Sacks, Alvin H.: Aerodynamic Forces, Moments, and Stability Derivatives for Slender Bodies of General Cross Section. NACA TN 3283, 1954.
15. Heaslet, Max. A., Lomax, Harvard, and Jones, Arthur L.: Volterra's Solution of the Wave Equation As Applied to Three-Dimensional Supersonic Airfoil Problems. NACA Rep. 889, 1947. (Supersedes NACA TN 1412.)
16. Bird, John D.: Some Theoretical Low-Speed Span Loading Characteristics of Swept Wings in Roll and Sideslip. NACA Rep. 969, 1950. (Supersedes NACA TN 1839.)
17. DeYoung, John: Theoretical Antisymmetric Span Loading for Wings of Arbitrary Plan Form at Subsonic Speeds. NACA Rep. 1056, 1951. (Supersedes NACA TN 2140.)
18. Malvestuto, Frank S., Jr., Margolis, Kenneth, and Ribner, Herbert S.: Theoretical Lift and Damping in Roll at Supersonic Speeds of Thin Sweptback Tapered Wings With Streamwise Tips, Subsonic Leading Edges, and Supersonic Trailing Edges. NACA Rep. 970, 1950. (Supersedes NACA TN 1860.)
19. Martin, John C., and Jeffreys, Isabella: Span Load Distributions Resulting From Angle of Attack, Rolling, and Pitching for Tapered Sweptback Wings With Streamwise Tips - Supersonic Leading and Trailing Edges. NACA TN 2643, 1952.
20. Mangler, K. W.: Calculation of the Pressure Distribution Over a Wing at Sonic Speeds. R. & M. No. 2888, British A.R.C., Sept. 1951.

TABLE I

MASS CHARACTERISTICS

	Pulsed horizontal-tail model	Pulsed rudder model
W, lb	155.5	158.5
I_x , slug-ft ²	1.106	0.942
I_y , slug-ft ²	9.06	9.73
I_z , slug-ft ²	9.92	10.60
I_{xz} , slug-ft ²	0.168	0.372
ϵ , deg	1.10	2.20
Center of gravity, percent \bar{c}	25.90	26.08

TABLE II
 ESTIMATED ACCURACY OF BASIC MEASUREMENTS
 FOR PULSED RUDDER MODEL

	Accuracy at Mach number of -	
	1.05	1.47
W, percent	0.7	0.7
I_Z , percent	2	2
I_X , percent	4	4
M, percent	2	1
q, percent	6	4
p/β , percent	2	2
$\frac{a_t/g}{\beta}$, percent	2	2
Ω_p , deg	3	3
ϵ , deg	0.5	0.5
P, sec	0.02	0.01
a, l/sec	0.10	0.05
λ_1 , percent	4	4

TABLE III

CALCULATED ACCURACY OF PARAMETERS

Due to estimated error in -	$\Delta C_{Y\beta}$		ΔC_{Lp}		$\Delta C_{n\beta}$		$\Delta C_{L\beta}$		$\Delta(C_{n_r} - C_{n\beta})$		$\Delta(C_{L_r} - C_{L\beta})$	
	M = 1.47	M = 1.05	M = 1.47	M = 1.05	M = 1.47	M = 1.05	M = 1.47	M = 1.05	M = 1.47	M = 1.05	M = 1.47	M = 1.05
W	0.008	0.008	-----	-----	0	0	0	0	0	0.010	0	0
I _Z	-----	-----	-----	-----	.006	.012	-----	-----	.027	.024	-----	-----
I _X	-----	-----	0.014	0.015	-----	-----	.006	.006	-----	-----	0	0
q	.053	.072	.016	.021	.003	.010	.004	.006	.100	.110	.043	.008
$\left \frac{p}{\beta} \right $	-----	-----	-----	-----	.001	.020	.002	.001	0	.010	.008	0
$\left \frac{a_t}{g} \right $.026	.026	-----	-----	0	0	0	0	0	0	0	0
Ω_p	-----	-----	-----	-----	.001	.014	.001	.001	.060	.070	.130	.140
e	-----	-----	0	0	.012	.012	.003	.006	0	0	.011	0
P	-----	-----	-----	-----	.025	.067	.005	.008	.020	.020	.015	.001
a	-----	-----	-----	-----	.002	.007	0	0	.030	.140	.002	0
λ_1	-----	-----	.002	.014	-----	-----	-----	-----	-----	-----	-----	-----
Probable error, $\sqrt{\Sigma \Delta^2}$	0.059	0.077	0.0214	0.0294	0.029	0.074	0.0096	0.0013	0.122	0.194	0.138	0.140
Value of derivative	-1.272	-1.358	-.334	-.370	.380	.600	-.103	-.105	-1.58	-1.37	.20	-.425
Probable error, percent of derivative	4.63	5.68	6.41	7.95	7.63	12.38	9.30	12.38	7.72	14.16	69	33
Due to - 100-percent change in C_{n_p}	-----	-----	-----	-----	0.003	0	-----	-----	0.390	0.290	-----	-----
Maximum probable error in C_{Lp}	-----	-----	-----	-----	-----	-----	0.0005	0	-----	-----	0.06	0.05

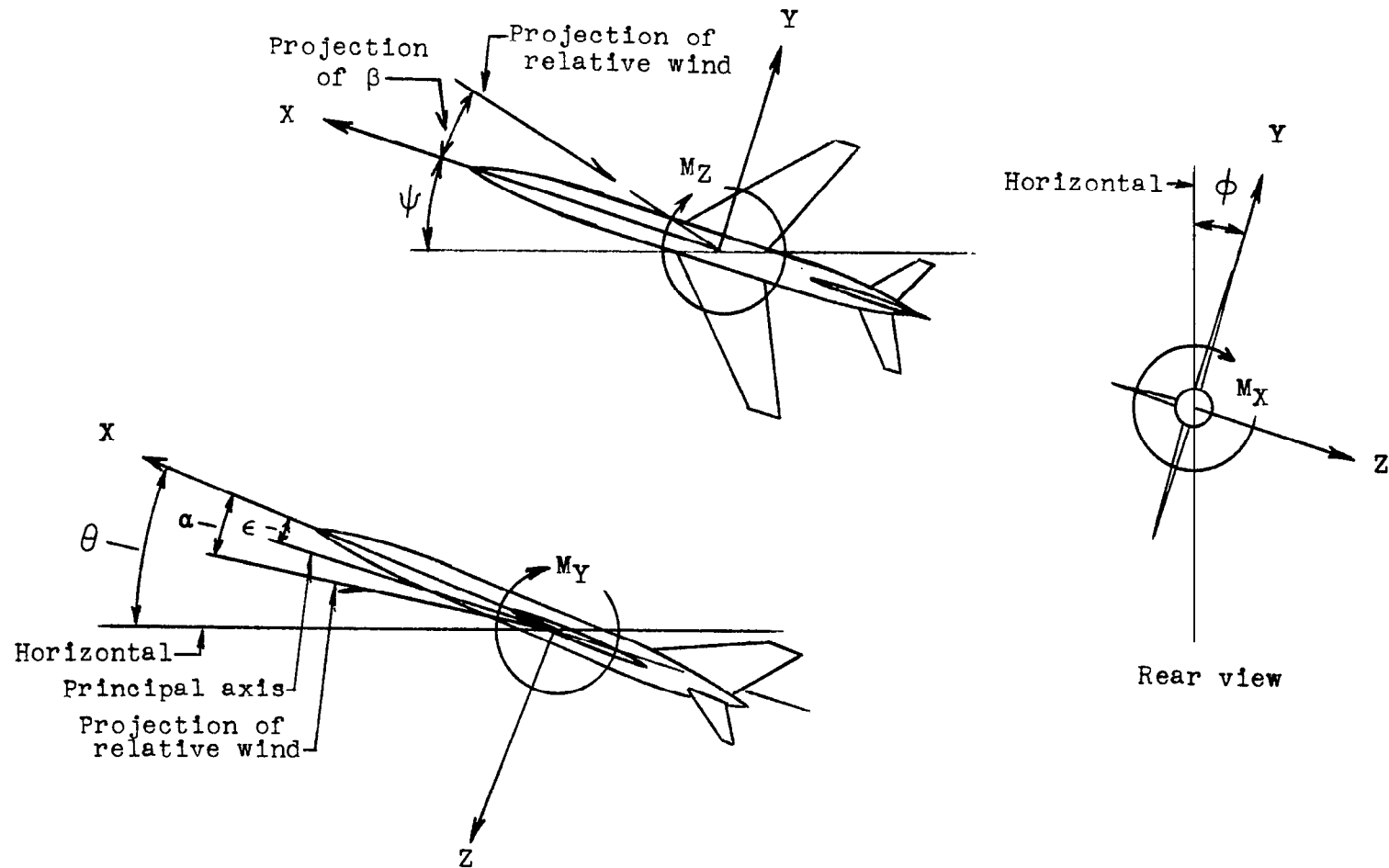
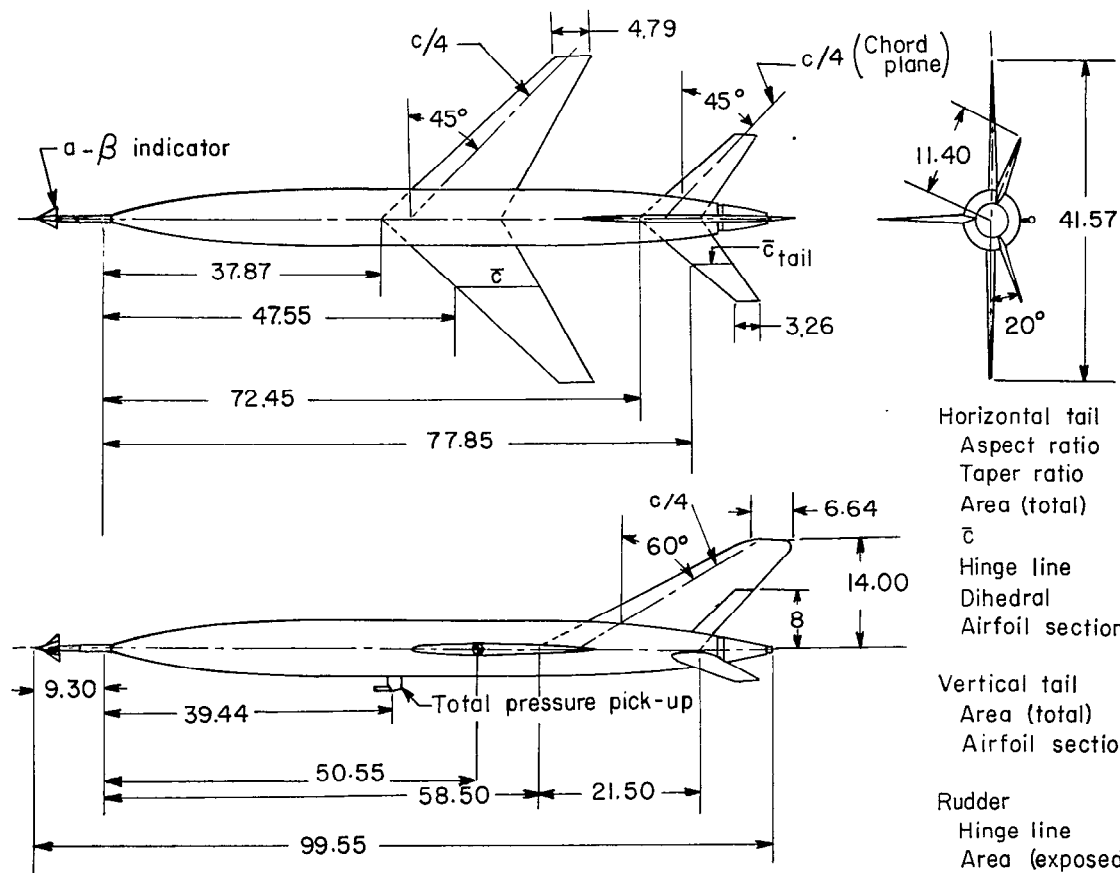
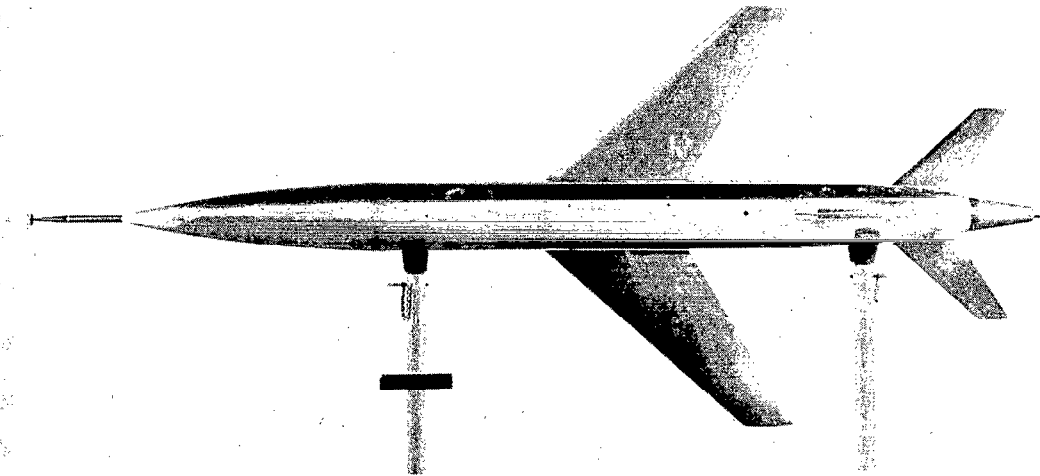


Figure 1.- System of axes. Each view presents a plane of axes system viewed along positive direction of third. Angular displacements as shown are positive. The center of gravity of model is at 25 percent of wing \bar{c} .

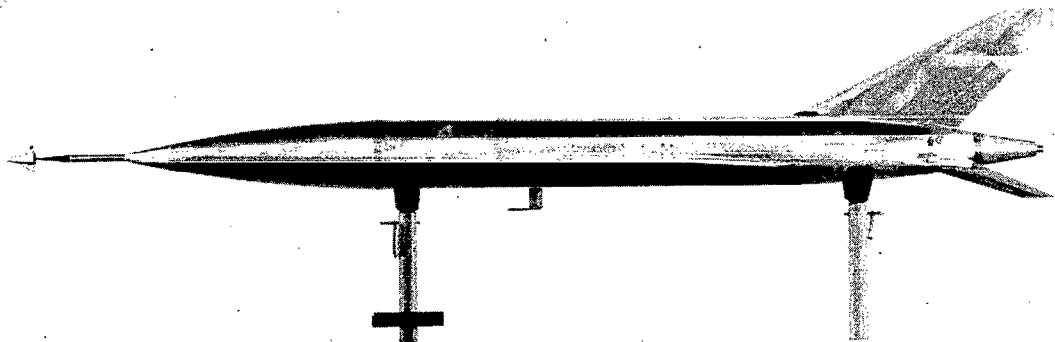


Horizontal tail	
Aspect ratio	4.00
Taper ratio	0.40
Area (total)	0.905 sq ft
\bar{c}	0.504 ft
Hinge line	0.42 chord
Dihedral	-20.00 deg
Airfoil section	NACA 65A 006
Vertical tail	
Area (total)	1.37 sq ft
Airfoil section	NACA 65A 003
Rudder	
Hinge line	0.80 chord
Area (exposed)	.13 sq ft
Wing	
Aspect ratio	4.00
Taper ratio	0.30
Area (total)	3.00 sq ft
\bar{c}	0.95 ft
Airfoil section	NACA 65A 006

Figure 2.- General arrangement of rudder model. All dimensions in inches.



Top view

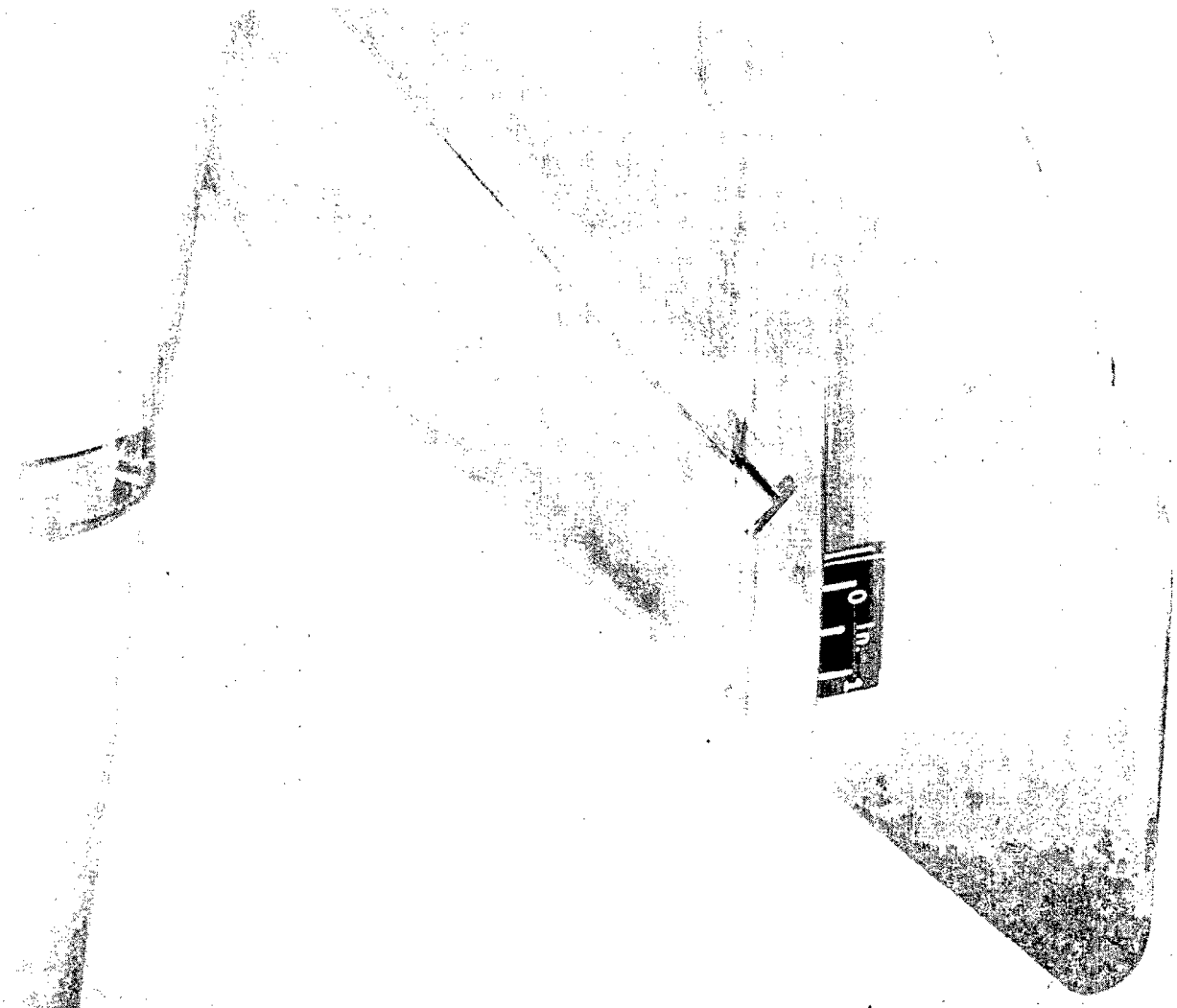


Side view

(a) Pulsed rudder model.

L-57-2716

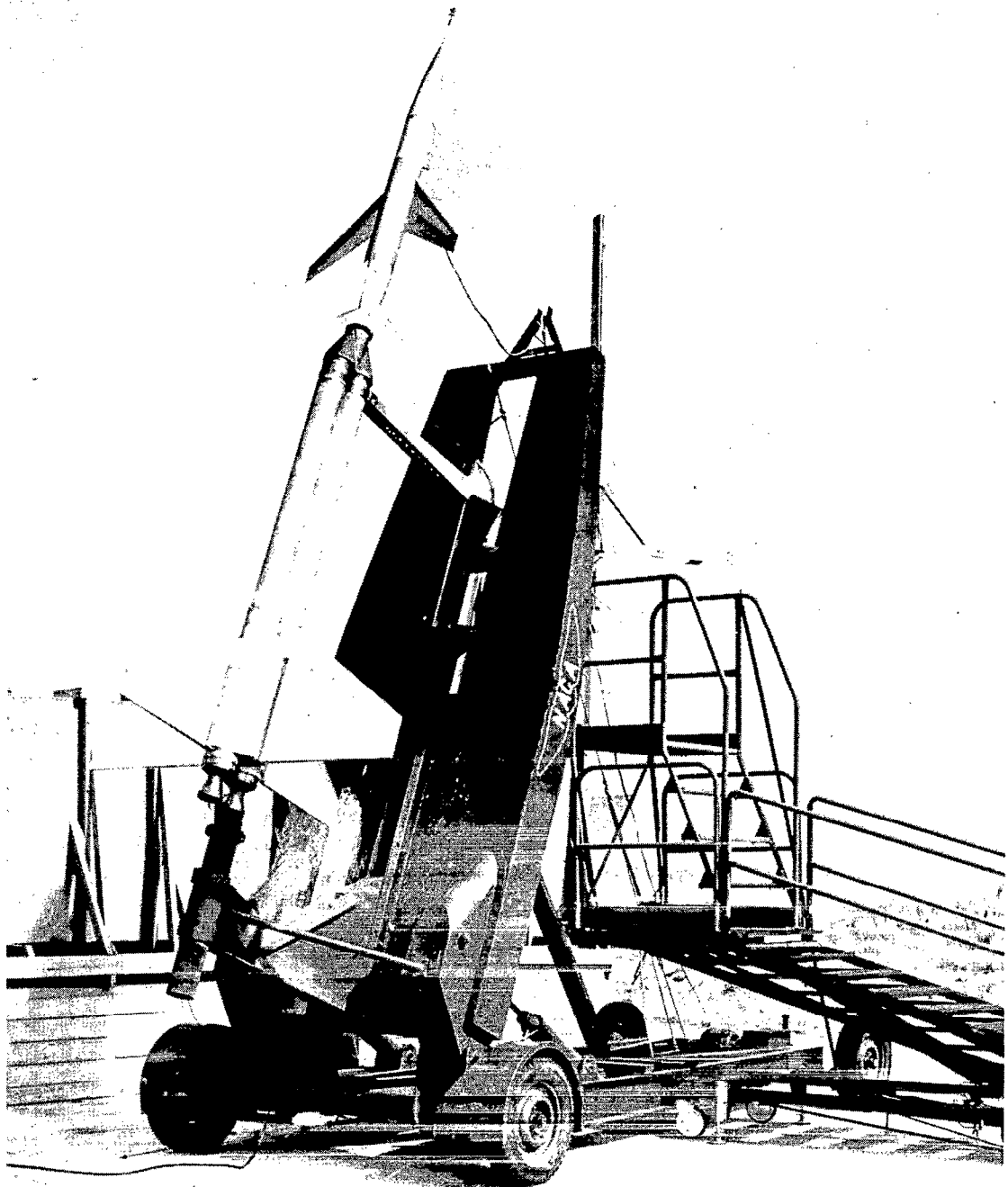
Figure 3.- Photographs of model and boost system.



(b) Pulsed rudder.

L-88448.1

Figure 3.- Continued.



L-88745.1

(c) Pulsed rudder model on booster in launching position.

Figure 3.- Concluded.

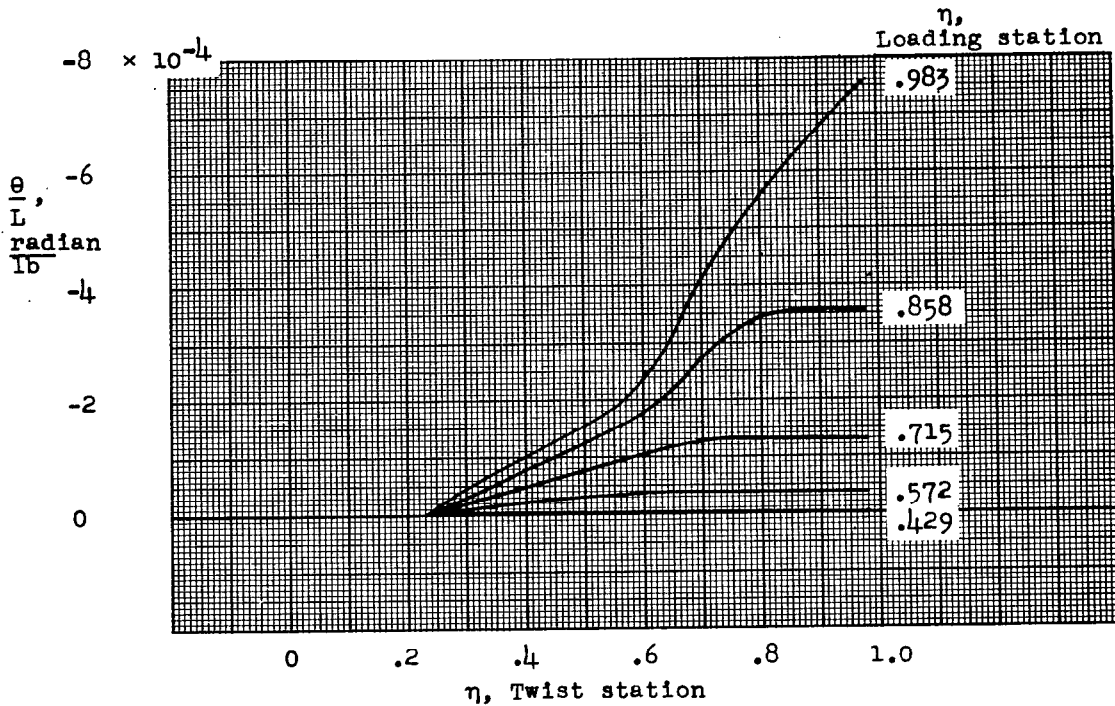


Figure 4.- Structural influence coefficients for vertical tail for loading along 0.40 chord line.

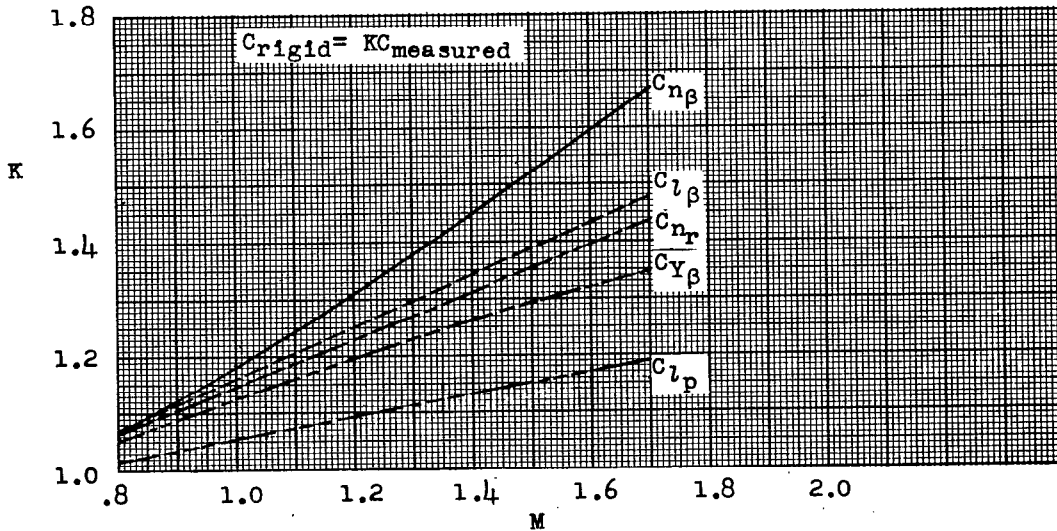
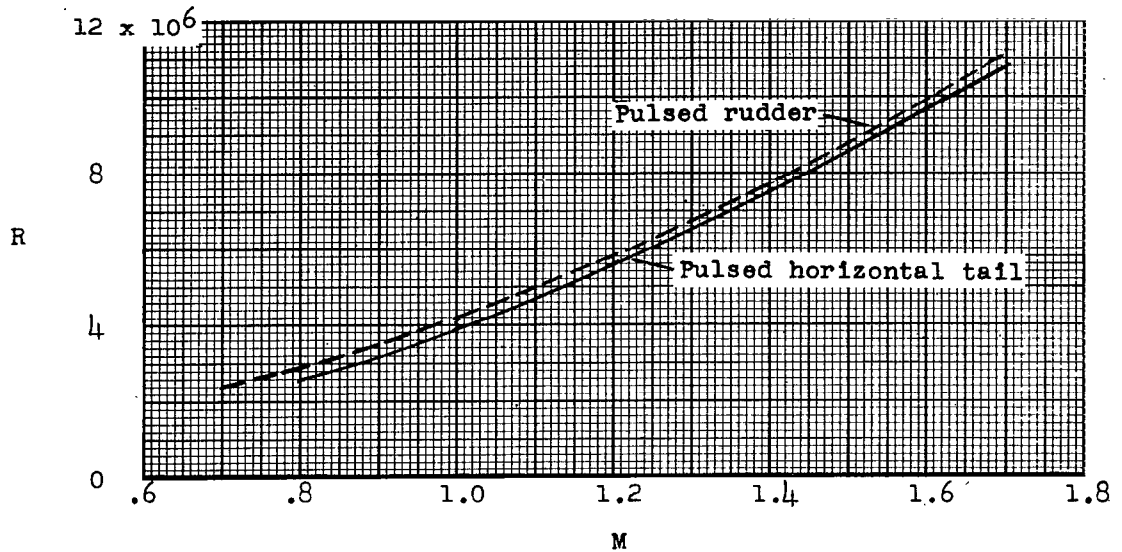
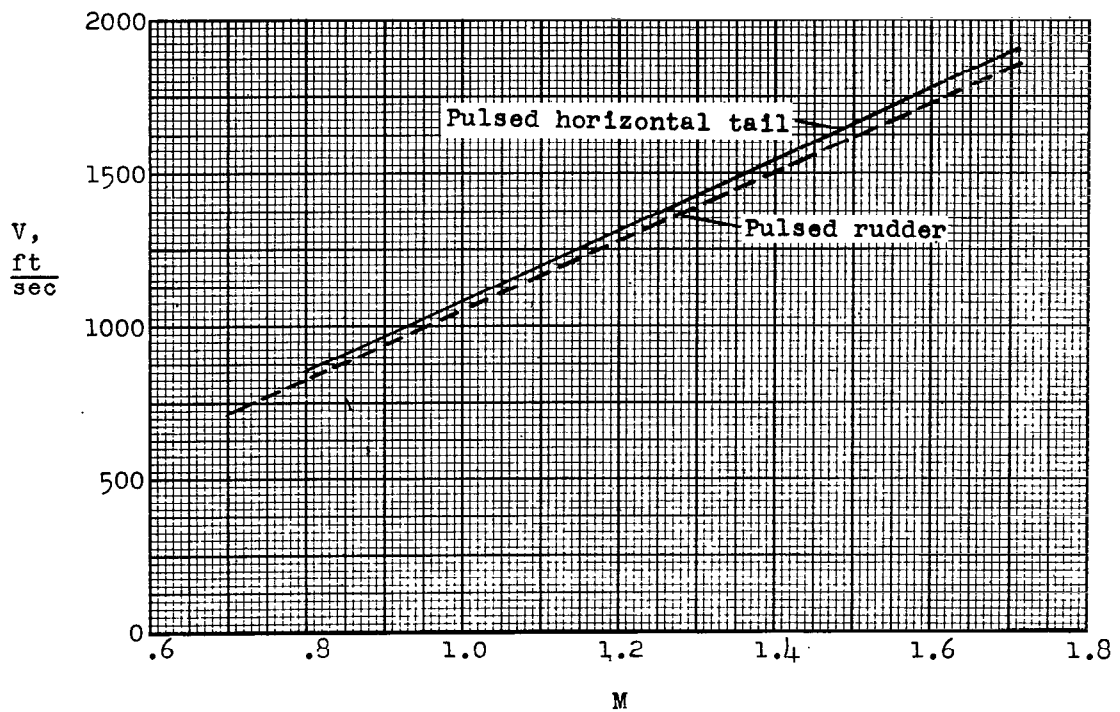


Figure 5.- Ratio of estimated rigid derivatives to estimated elastic derivatives.

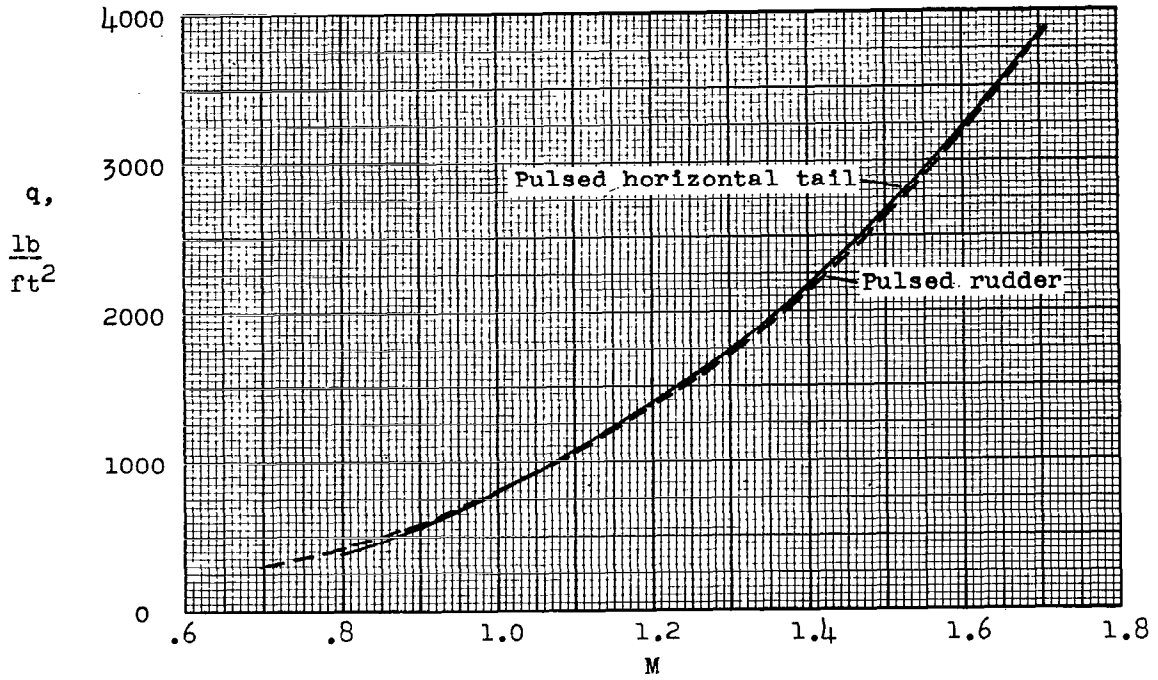


(a) Reynolds number based on wing mean aerodynamic chord.

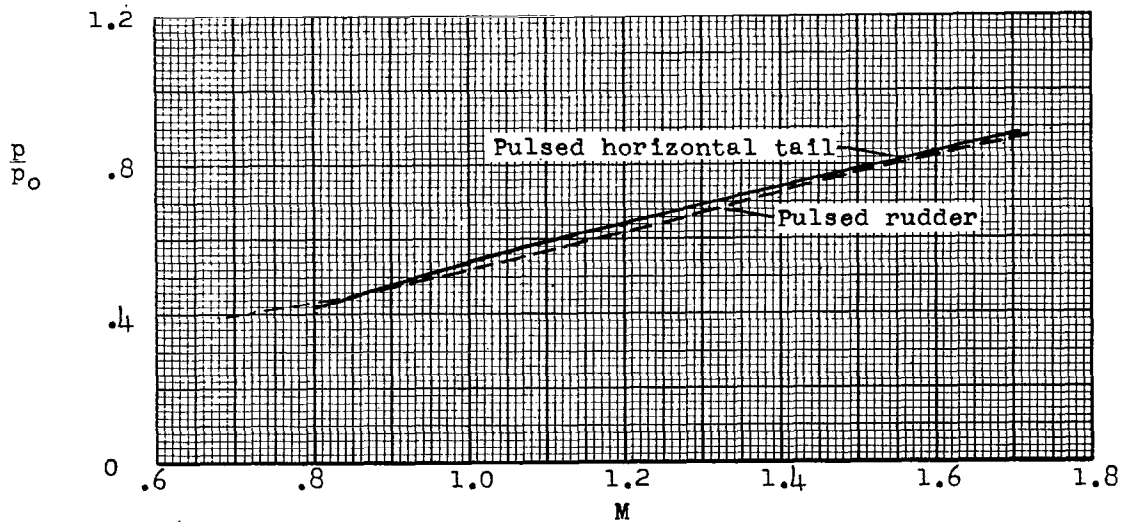


(b) Velocity.

Figure 6.- Flight test conditions.

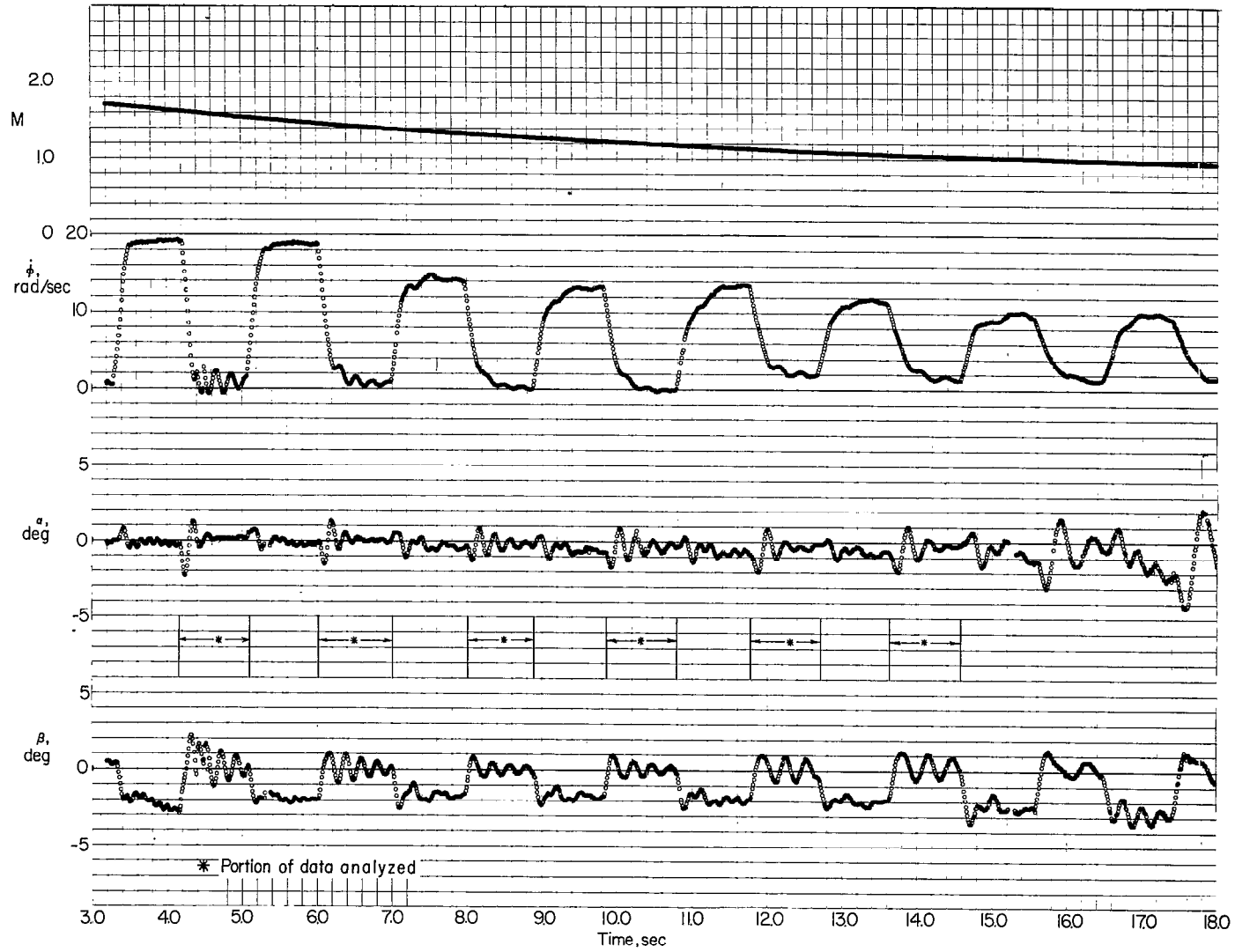


(c) Dynamic pressure.



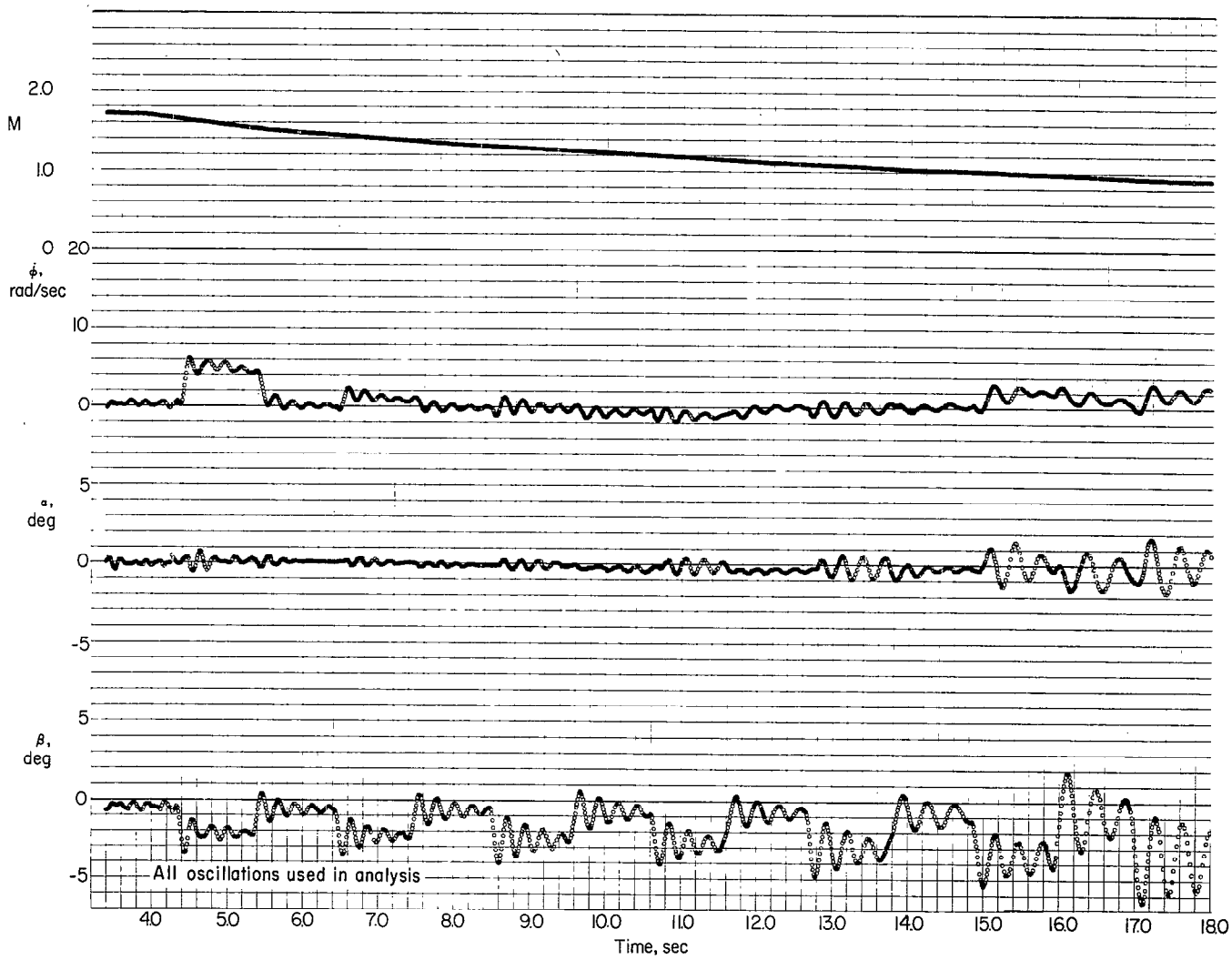
(d) Static pressure ratio.

Figure 6.- Concluded.



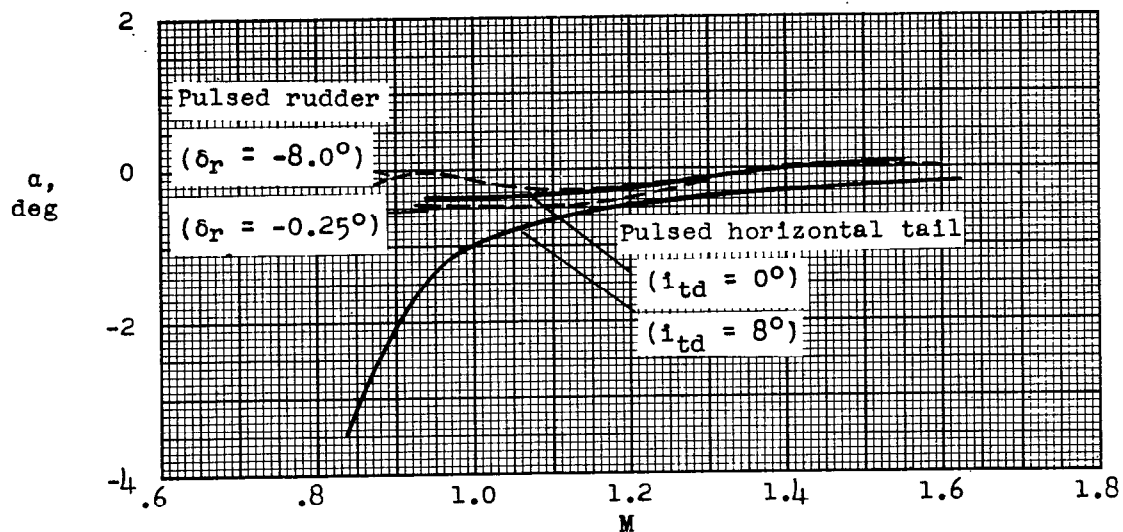
(a) Differentially pulsed horizontal-tail model.

Figure 7.- Portion of time history.

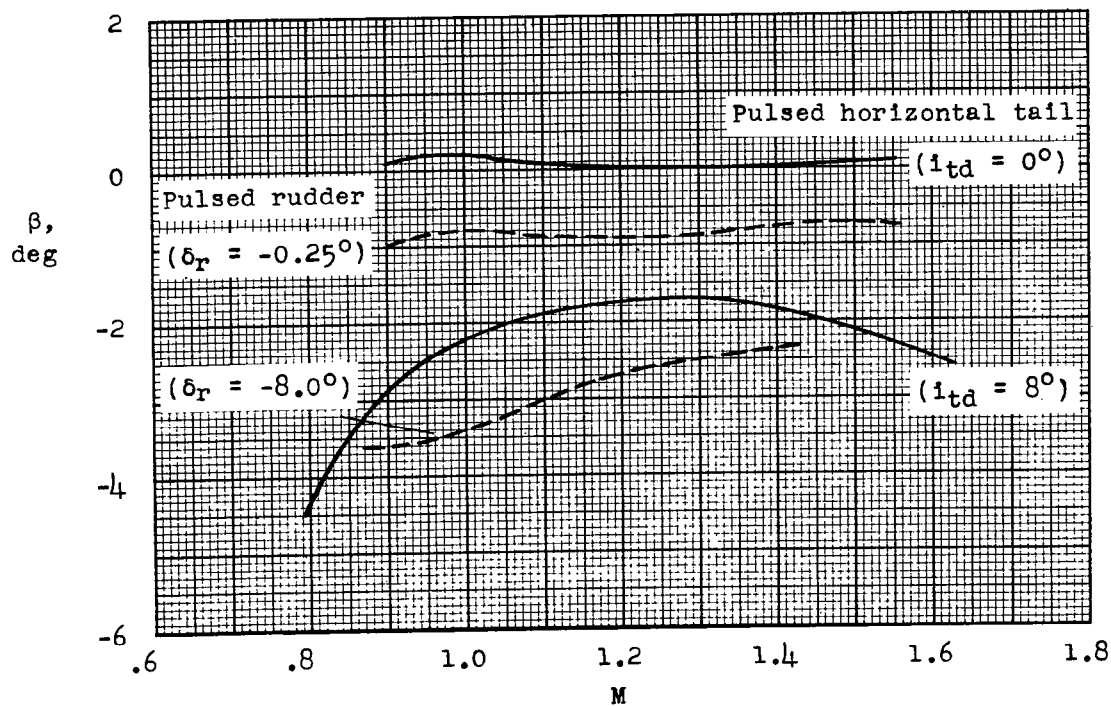


(b) Pulsed rudder model.

Figure 7.- Concluded.

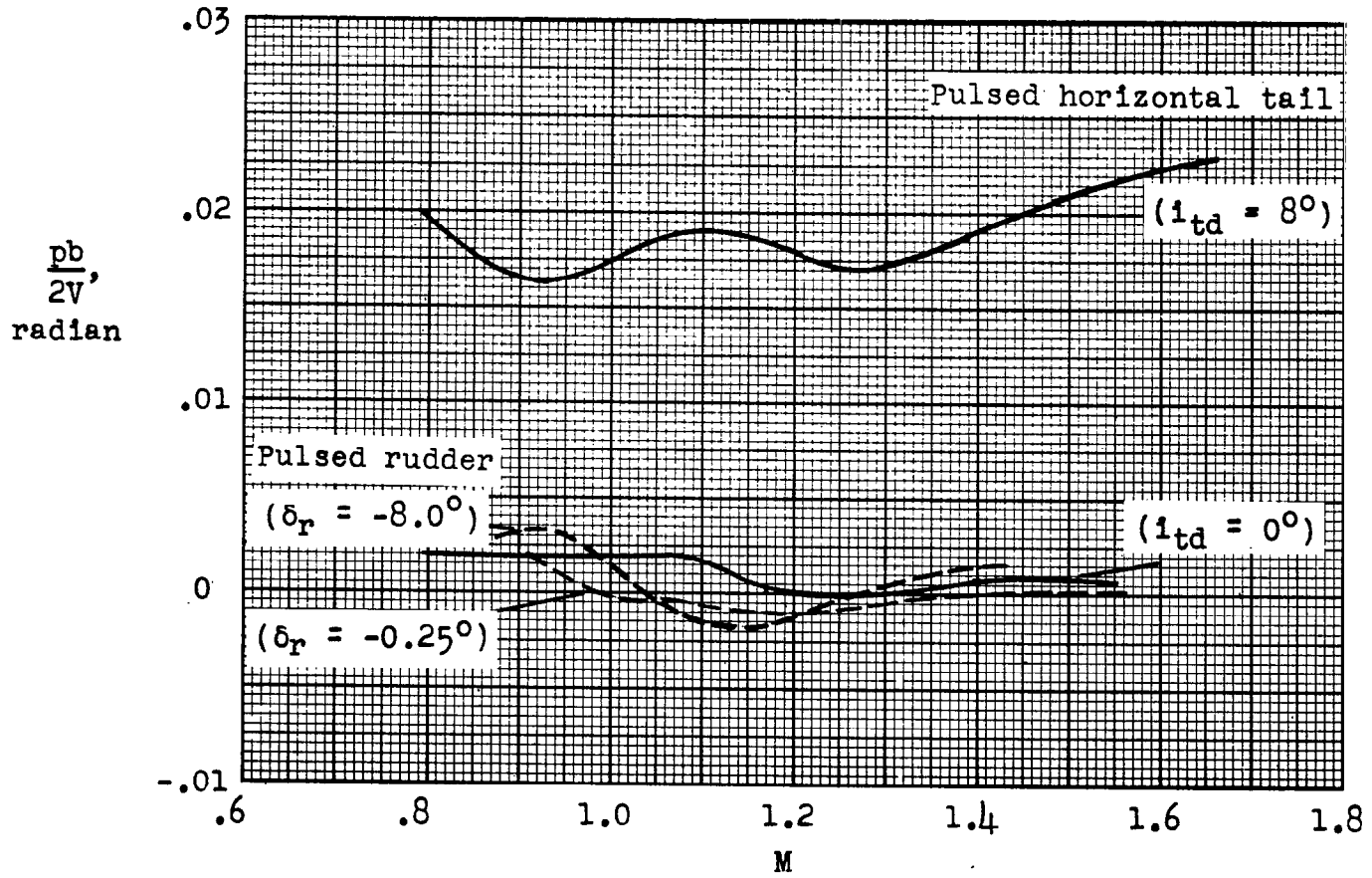


(a) Angle of attack.



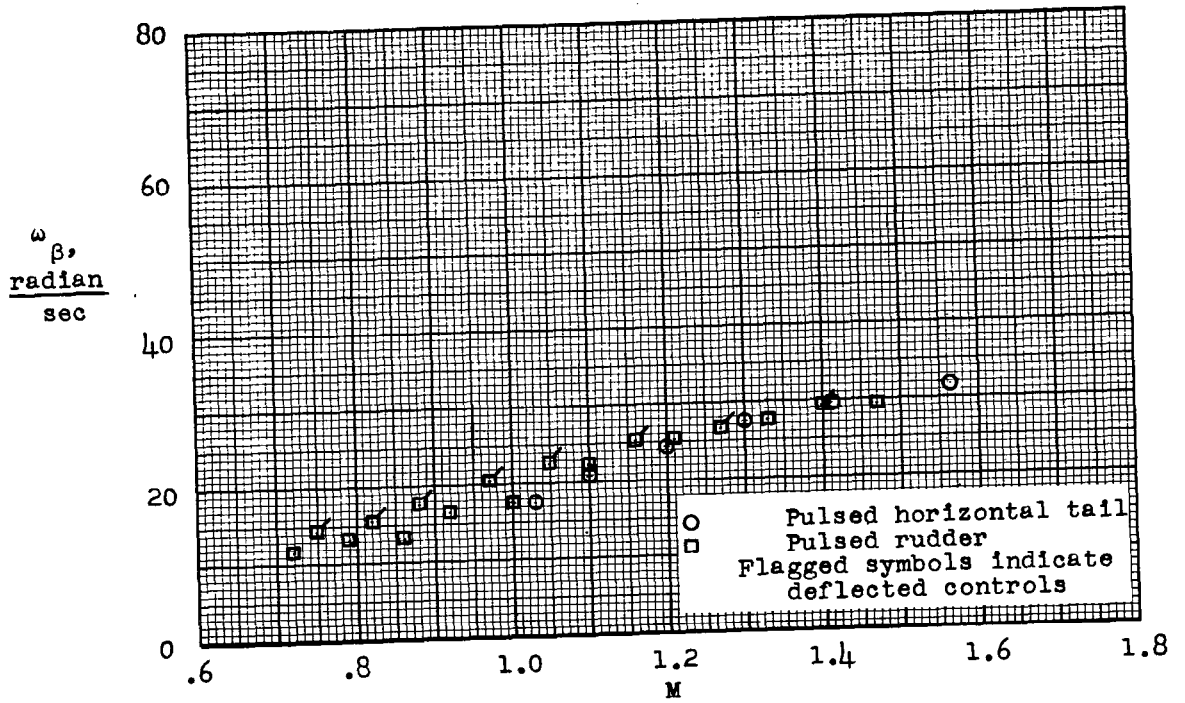
(b) Angle of sideslip.

Figure 8.- Variation of trim conditions with Mach number.

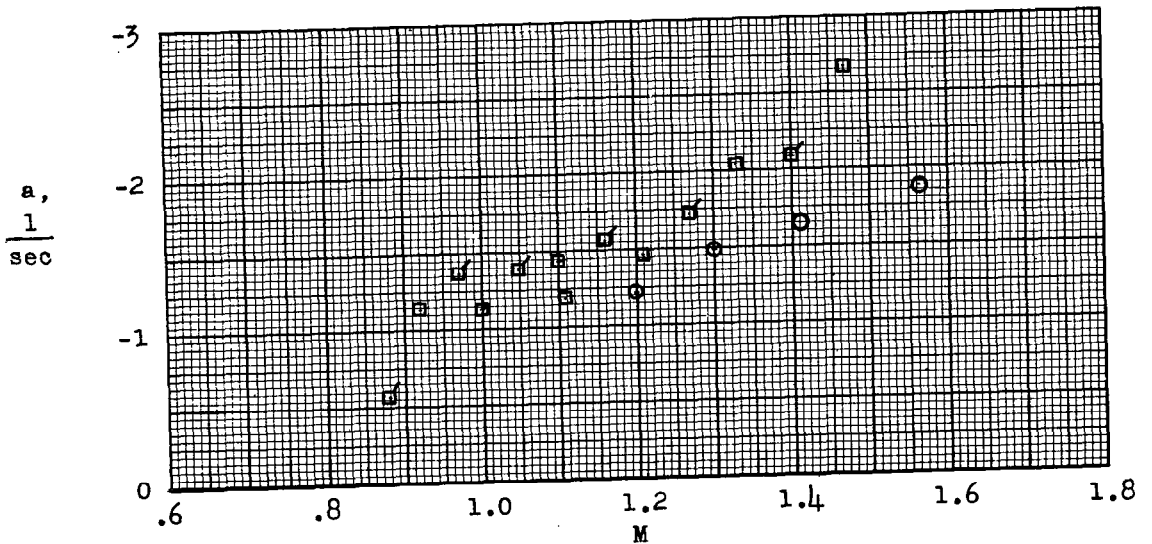


(c) Rolling parameter.

Figure 8.- Concluded.

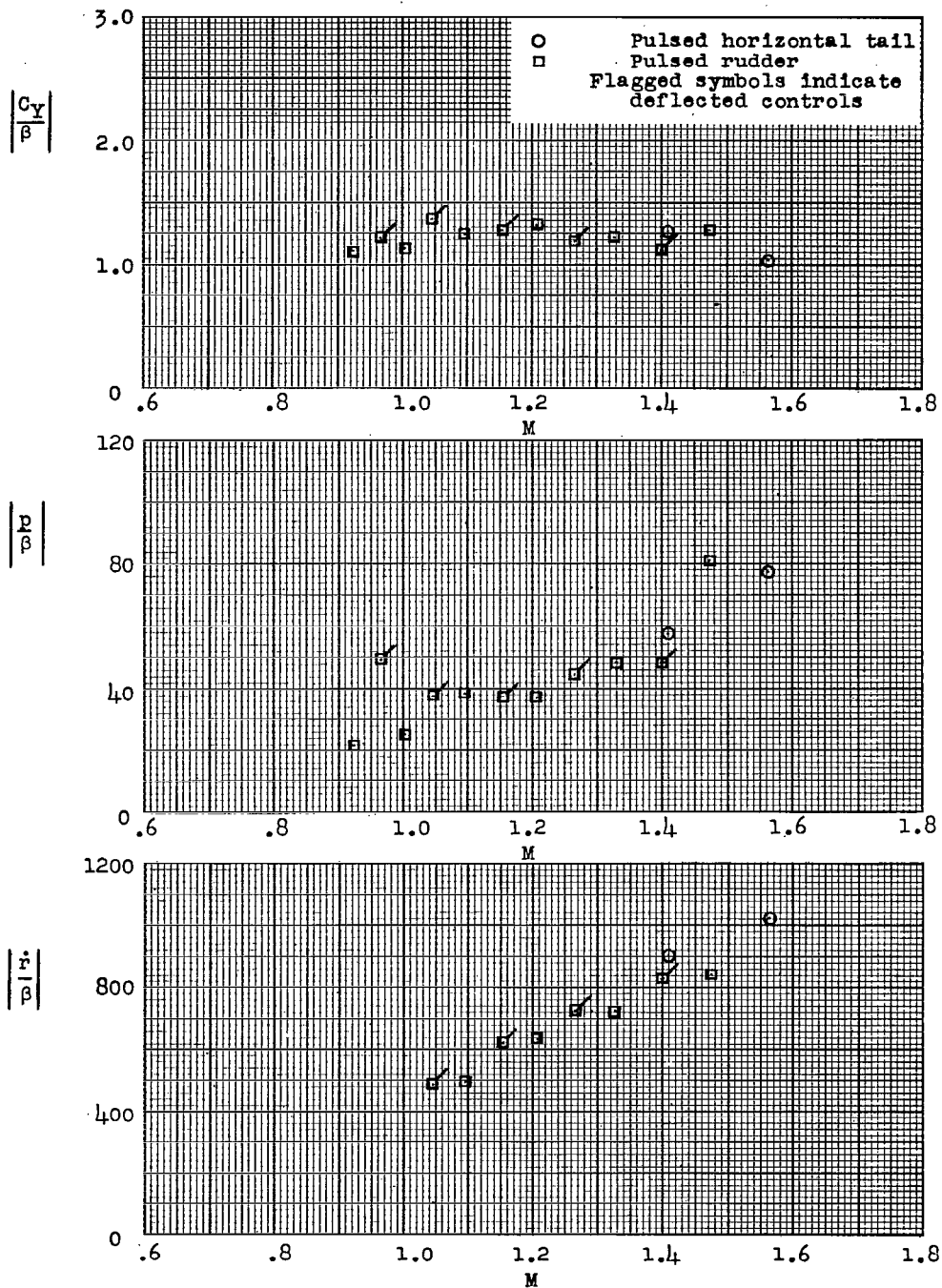


(a) Frequency.



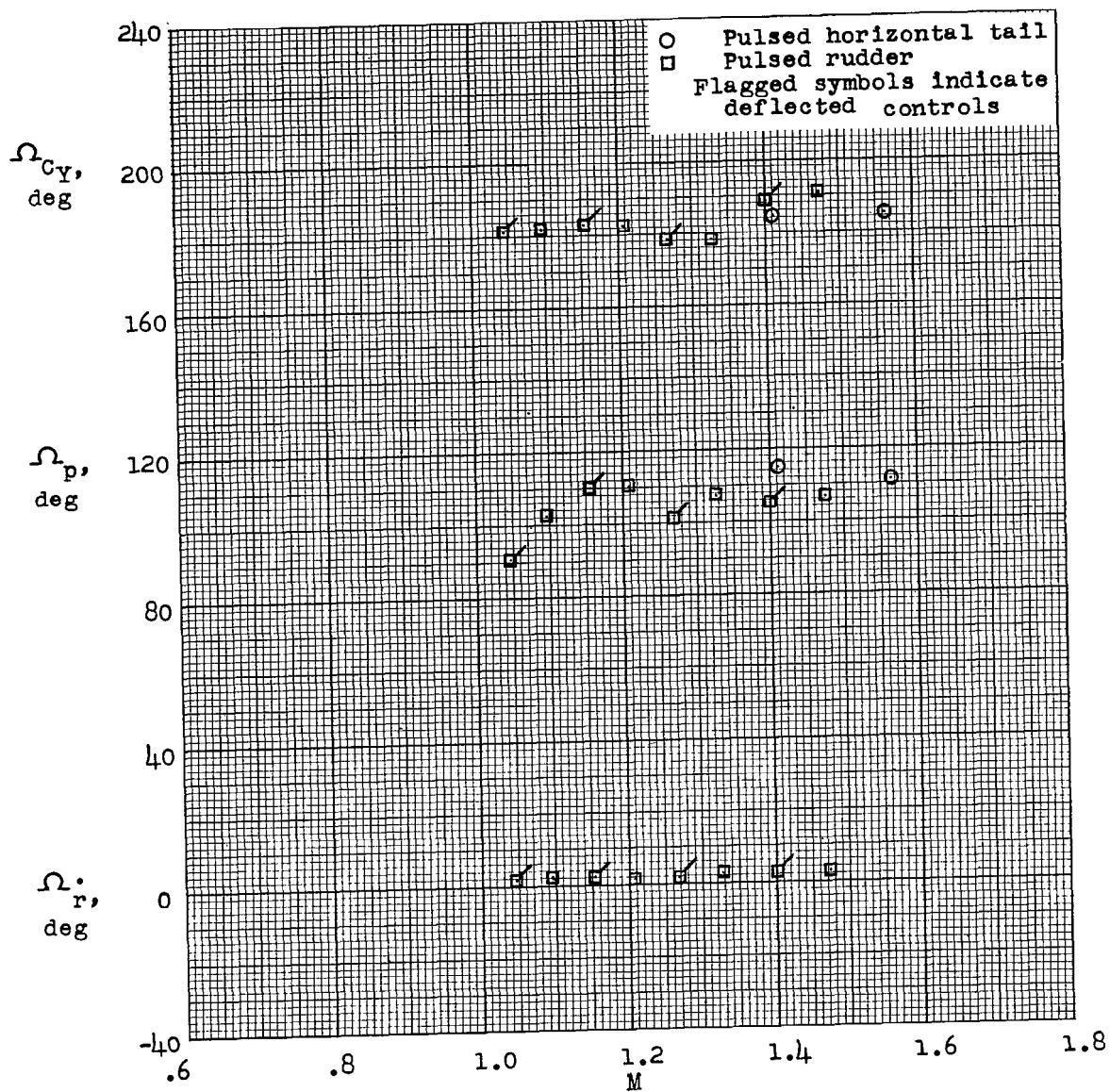
(b) Damping factor.

Figure 9.- Characteristics of lateral oscillations.



(c) Amplitude ratios.

Figure 9.- Continued.



(d) Phase angles.

Figure 9.- Concluded.

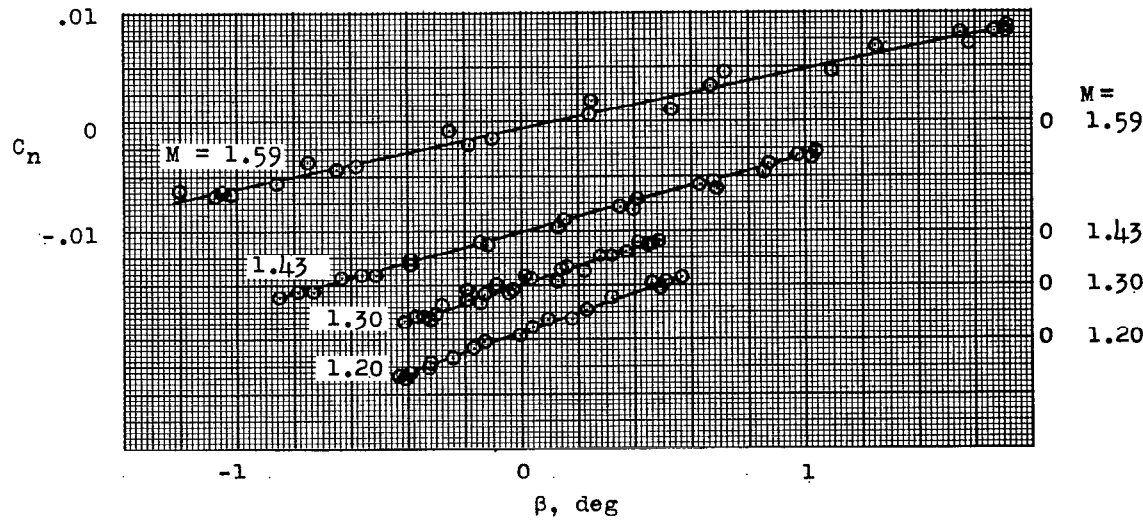
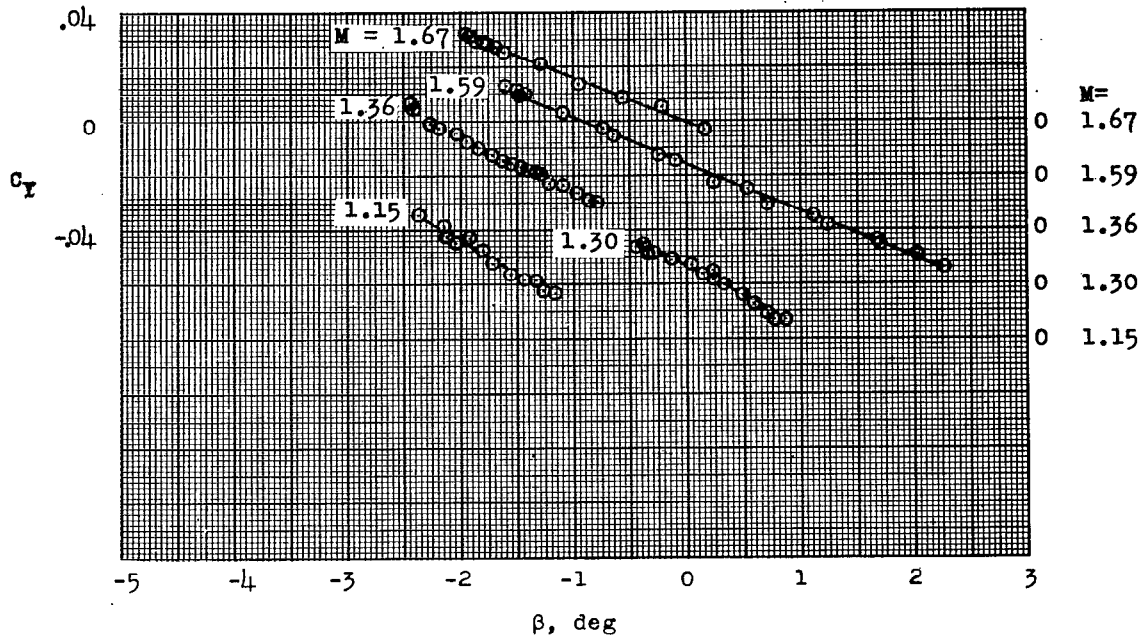


Figure 10.- Typical experimental variation of lateral-force and yawing-moment coefficients with angle of sideslip and Mach number for pulsed horizontal-tail model.

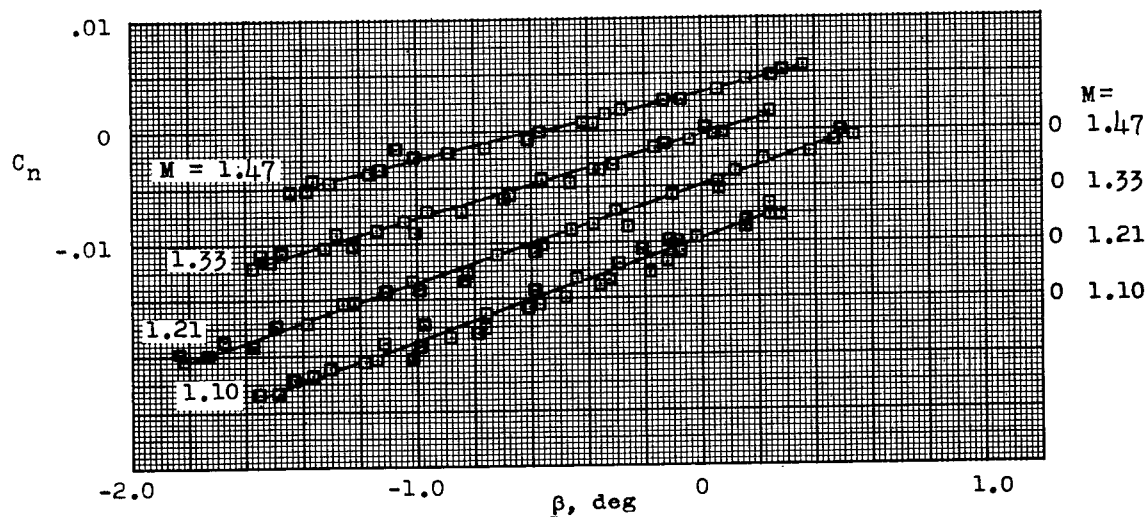
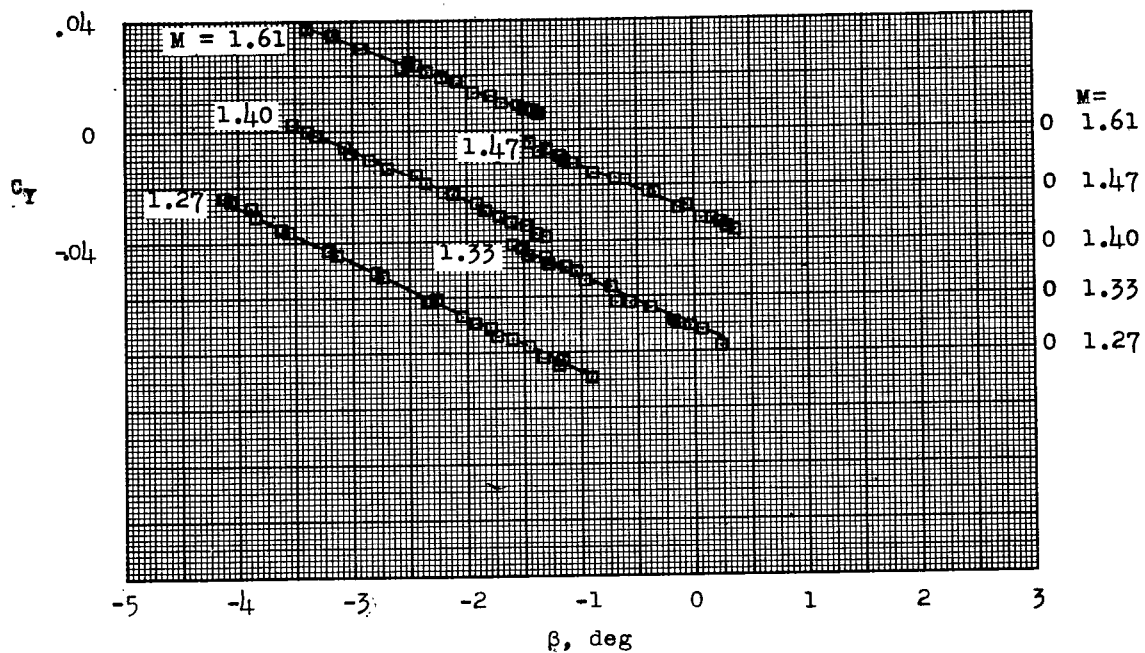


Figure 11.- Typical experimental variation of lateral-force and yawing-moment coefficients with angle of sideslip and Mach number for pulsed rudder model.

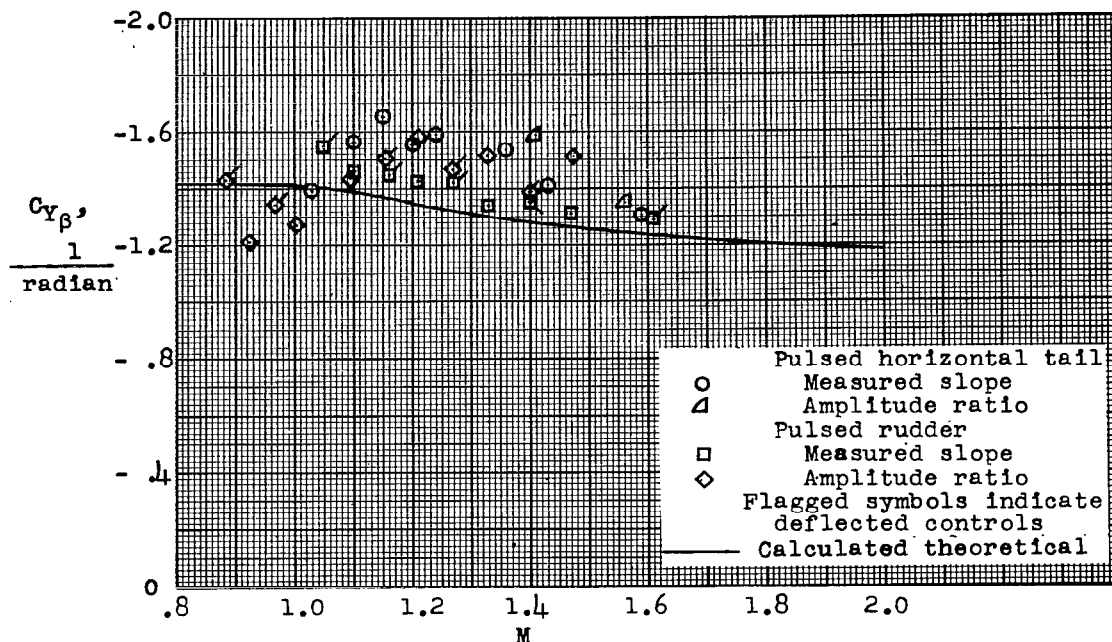


Figure 12.- Variation of lateral force due to sideslip derivative $C_{Y\beta}$ with Mach number for rigid conditions.

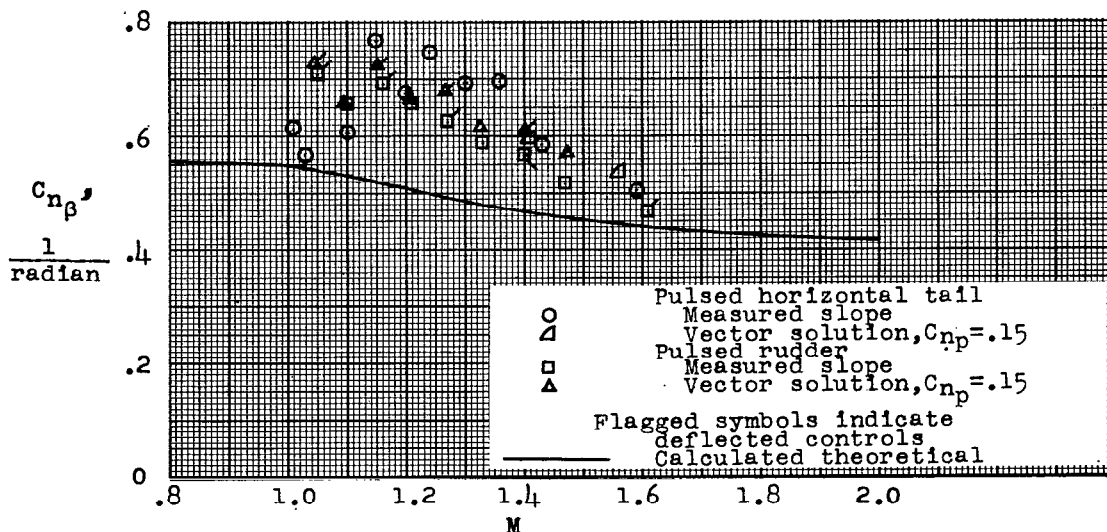


Figure 13.- Variation of the static directional stability derivative $C_{n\beta}$ with Mach number for rigid conditions.

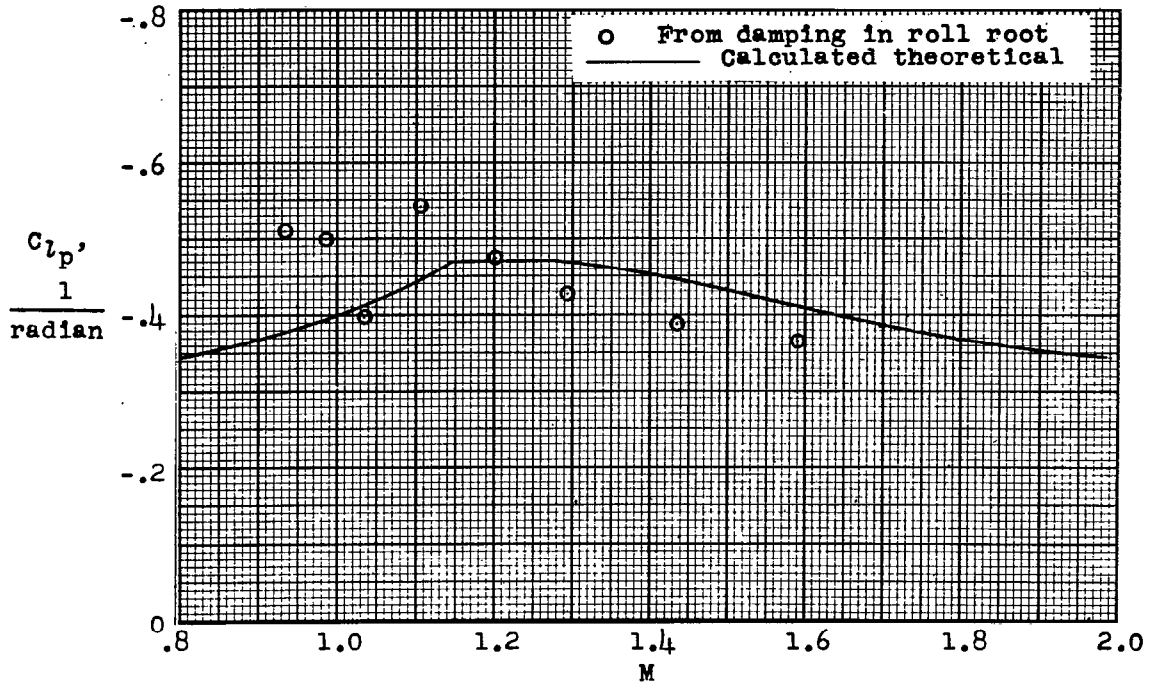


Figure 14.- Variation of damping-in-roll derivative C_{l_p} with Mach number for rigid conditions.

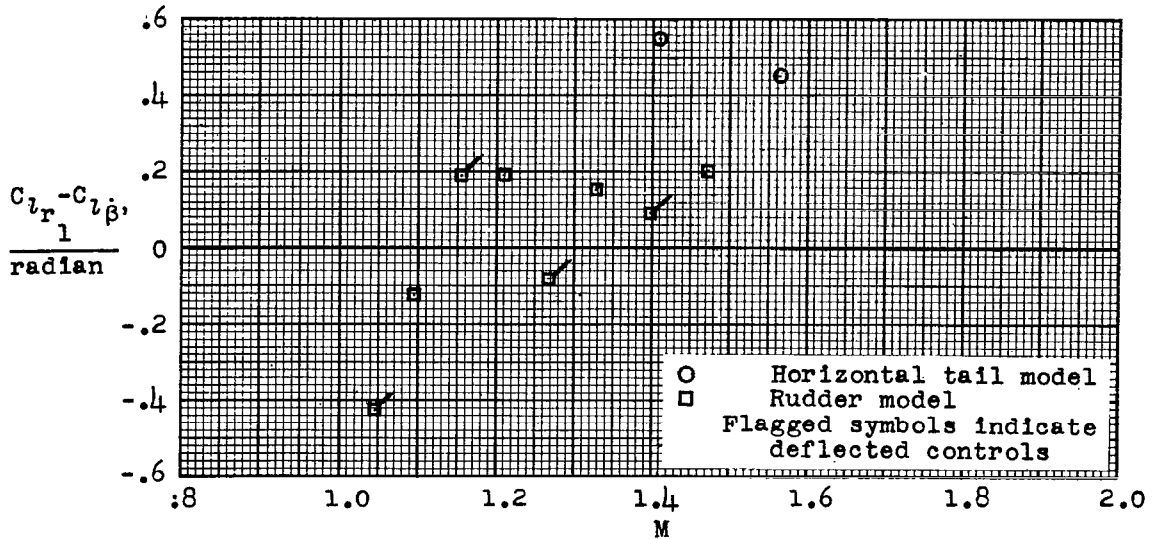


Figure 15.- Variation of lateral stability derivative $C_{l_r} - C_{l_{\beta}}$ with Mach number.

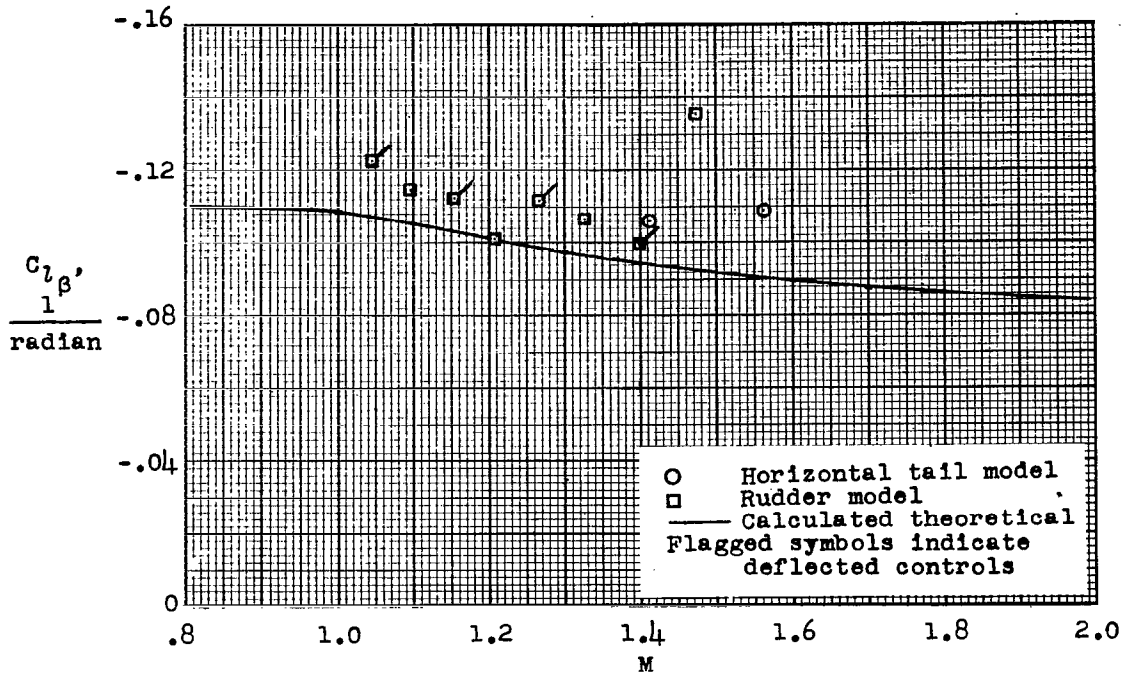


Figure 16.- Variation of effective dihedral derivative $C_{l\beta}'$ with Mach number for rigid conditions.

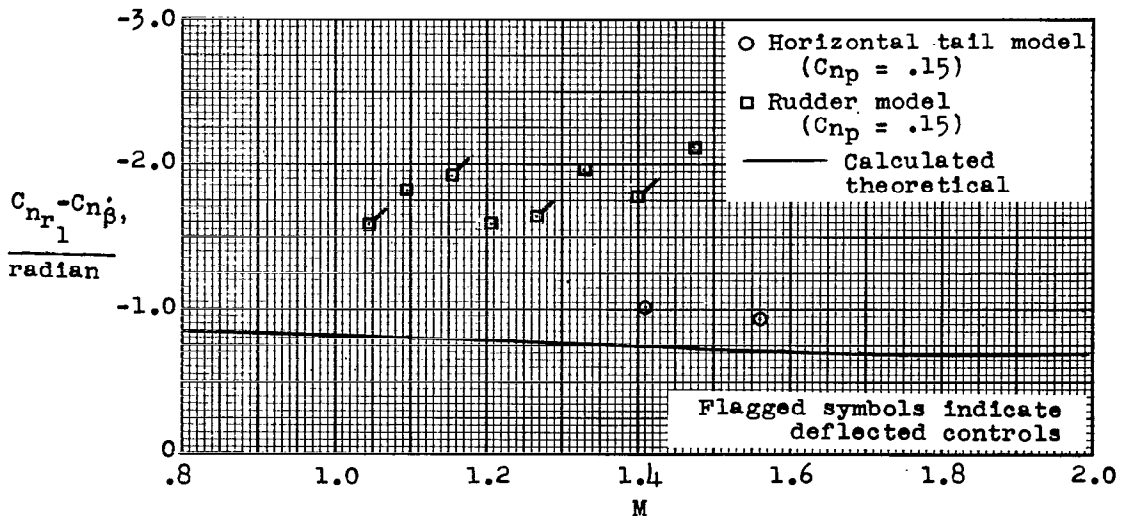
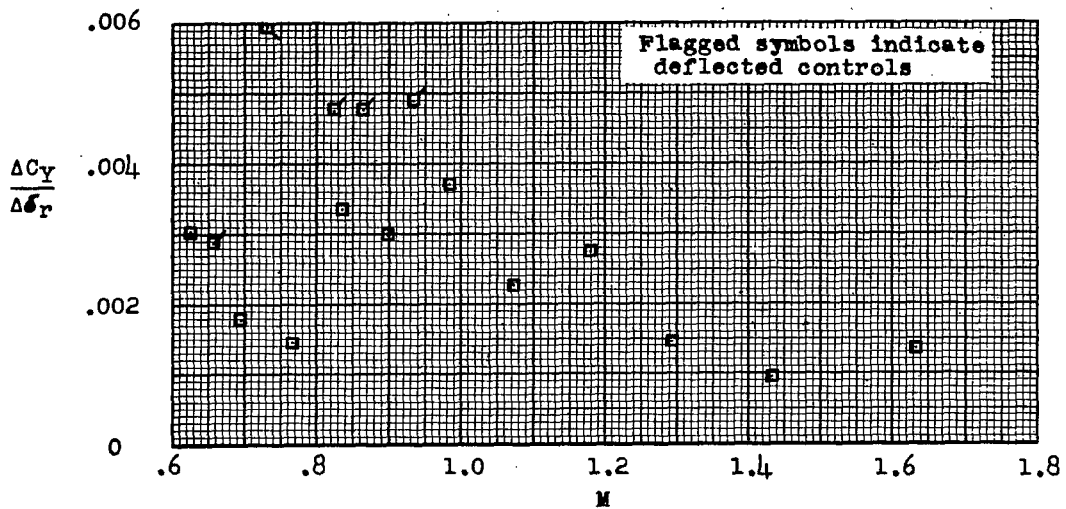
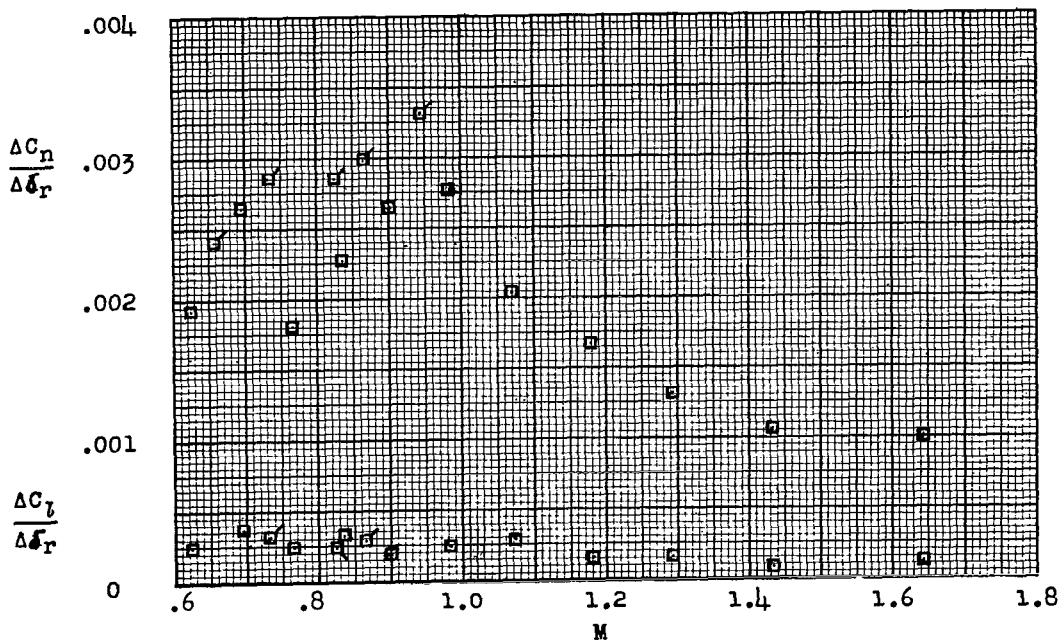


Figure 17.- Variation of damping-in-yaw derivative C_{nr} with Mach number for rigid conditions.



(a) Variation with Mach number of change in lateral-force coefficient due to abrupt rudder deflection.



(b) Variation with Mach number of yawing moment effectiveness, $\frac{\Delta C_n}{\Delta \delta_r}$, and rolling moment effectiveness, $\frac{\Delta C_l}{\Delta \delta_r}$ for pulsed rudder model.

Figure 18.- Control effectiveness of pulsed rudder.

NASA Technical Library



3 1176 01438 1173



CONFIDENTIAL